Correction of pathlength amplification in the filter-pad technique for measurements of particulate absorption coefficient in the visible spectral region

ARTICLE *in* APPLIED OPTICS · SEPTEMBER 2015

Impact Factor: 1.78 · DOI: 10.1364/AO.54.006763

applied optics

Correction of pathlength amplification in the filter-pad technique for measurements of particulate absorption coefficient in the visible spectral region

Dariusz Stramski,[1,*] Rick A. Reynolds,[1] Sławomir Kaczmarek,[2] Julia Uitz,[1,3] and Guangming Zheng[1,4,5]

[1]Marine Physical Laboratory, Scripps Institution of Oceanography, University of California San Diego, La Jolla, California 92093-0238, USA
[2]Institute of Oceanology, Polish Academy of Sciences, Powstancow Warszawy 55, 81-712 Sopot, Poland
[3]Currently at Sorbonne Universités, UPMC Université Paris 06, CNRS, Observatoire Océanologique de Villefranche (OOV), Laboratoire d'Océanographie de Villefranche (LOV), 181 Chemin du Lazaret, 06 230, Villefranche-sur-Mer, France
[4]Currently at NOAA/NESDIS/Center for Satellite Application and Research, 5830 University Research Court, College Park, Maryland 20740, USA
[5]Currently at Global Science & Technology, Inc., 7855 Walker Drive, Suite 200, Greenbelt, Maryland 20770, USA
*Corresponding author: dstramski@ucsd.edu

Received 2 April 2015; revised 26 June 2015; accepted 1 July 2015; posted 1 July 2015 (Doc. ID 237332); published 27 July 2015

Spectrophotometric measurement of particulate matter retained on filters is the most common and practical method for routine determination of the spectral light absorption coefficient of aquatic particles, $a_p(\lambda)$, at high spectral resolution over a broad spectral range. The use of differing geometrical measurement configurations and large variations in the reported correction for pathlength amplification induced by the particle/filter matrix have hindered adoption of an established measurement protocol. We describe results of dedicated laboratory experiments with a diversity of particulate sample types to examine variation in the pathlength amplification factor for three filter measurement geometries; the filter in the transmittance configuration (T), the filter in the transmittance-reflectance configuration (T-R), and the filter placed inside an integrating sphere (IS). Relationships between optical density measured on suspensions (OD_s) and filters (OD_f) within the visible portion of the spectrum were evaluated for the formulation of pathlength amplification correction, with power functions providing the best functional representation of the relationship for all three geometries. Whereas the largest uncertainties occur in the T method, the IS method provided the least sample-to-sample variability and the smallest uncertainties in the relationship between OD_s and OD_f. For six different samples measured with 1 nm resolution within the light wavelength range from 400 to 700 nm, a median error of 7.1% is observed for predicted values of OD_s using the IS method. The relationships established for the three filter-pad methods are applicable to historical and ongoing measurements; for future work, the use of the IS method is recommended whenever feasible.

OCIS codes: (010.1030) Absorption; (010.4450) Oceanic optics.

http://dx.doi.org/10.1364/AO.54.006763

1. INTRODUCTION

Spectrophotometric measurements of light absorption by aquatic particles collected on filters have long been the only method available for routine determinations of the spectral absorption coefficient of particles, $a_p(\lambda)$, with high spectral resolution (~1 nm) over a broad spectral range from the ultraviolet (UV) through visible (VIS) to near-infrared (NIR) (λ is light wavelength in vacuo). This method was pioneered over 50 years ago [1,2] and is generally referred to as the filter-pad technique. In this technique the particles are concentrated on a filter to overcome limitations of direct measurements on particle suspensions, which are associated with generally low particle concentrations in natural waters. Trüper and Yentsch [3] proposed to measure the particulate absorption directly on wet glass-fiber filters with a conventional bench-top spectrophotometer, and since then this approach has been commonly employed in the filter-pad measurements. It is reasonable to expect that despite ongoing efforts to develop new techniques for absorption measurements in aquatic environments such as that based on the integrating cavity [4–6], the filter-pad technique is likely to

remain the main technique for measuring the high-spectral resolution particulate absorption coefficient over a broad spectral range for the foreseeable future. In addition to the determination of $a_p(\lambda)$, the filter-pad technique provides a capability to experimentally determine the phytoplankton, $a_{ph}(\lambda)$, and nonalgal particulate (often referred to as detrital or depigmented), $a_{NAP}(\lambda)$, components of $a_p(\lambda)$. This partitioning of $a_p(\lambda)$ is typically accomplished by treating the sample filter with organic solvent or bleaching agent in order to extract or bleach pigments present in phytoplankton cells [7,8]. The partitioning of $a_p(\lambda)$ can also be accomplished numerically with models [e.g., 9–11].

The particulate absorption coefficient, $a_p(\lambda)$, and its components $a_{ph}(\lambda)$ and $a_{NAP}(\lambda)$, are highly variable in the world's oceans. The accurate quantification of these coefficients and their variability is important to many questions in the fields of ocean optics, physics, biology, and biogeochemistry, as well as various applications of optical measurements to oceanographic studies. For example, the absorption data carry information about various water constituents and processes in the ocean, such as phytoplankton pigments, taxonomic composition, and size structure of phytoplankton communities, photosynthesis, and primary production, as well as heat transfer in the upper water column [e.g., 12–16]. The absorption coefficient of seawater including the particulate component is also a major determinant of spectral remote-sensing reflectance of the ocean, $R_{rs}(\lambda)$, and can be estimated from satellite imagery of ocean color [e.g., 17–20]. Methodological advances toward achieving the highest possible accuracy in field determinations of particulate absorption coefficient with high spectral resolution are particularly relevant to satellite missions planned for the near future, such as the National Aeronautics and Space Administration (NASA) PACE (current acronym corresponds to Pre-Aerosol, Clouds, and ocean Ecosystem) mission which is anticipated to extend the spectral range and resolution of ocean color observations as compared to current and past satellite sensors. Such future missions will require improved field determinations of the absorption coefficient to reap the full benefits of these new remote-sensing capabilities through development of better algorithms and validation of satellite retrievals.

Improvements in the methodology of the filter-pad technique and the characterization of associated uncertainties have been the focus of many studies over the past few decades. Numerous sources of uncertainties have been reported including: the pathlength amplification resulting from light scattering within the sample/filter matrix, incomplete detection of light scattered by the sample, variations in filter wetness during the measurement, filter-to-filter variations in the optical properties of filters, effects associated with particle distribution and particle load on the filter, incomplete retention of particles on the filter, temporal instability of particulate absorption during the measurement, as well as additional potential problems related to sample handling, filtration, freezing, and storage procedures [e.g., 9,21–32].

Despite numerous studies devoted to the methodology of filter-pad technique and widespread use of this technique in aquatic science, the formulation of a consensus protocol for accurate quantification of the particulate absorption coefficient has remained elusive. The two most critical and consequential issues for the protocol and performance of the filter-pad technique are the geometrical configuration of the spectrophotometric measurement and the correction for pathlength amplification. Three distinctly different configurations of filter-pad measurements are transmittance (T) [2], transmittance-reflectance (T-R) [26], and inside an integrating sphere (IS) [23]. The T configuration has been most commonly used as a standard method since the inception of the filter-pad technique but suffers from a poor geometry of measurement in which a large fraction of scattered light is undetected by the spectrophotometer. This results in difficult-to-quantify potentially significant errors in the determinations of $a_p(\lambda)$. The T-R configuration largely circumvents these limitations, but this method is more laborious and has not been used routinely. The IS configuration represents the most desirable geometry of measurement ensuring the detection of nearly all photons scattered by the sample, but this technique has been used very rarely. Only over the last few years efforts have been increasing toward implementing the inside-sphere method in routine use of the filter-pad technique [32–34].

The pathlength amplification is associated with an increase in the pathlength that the photons travel within a scattering medium, which results in the enhancement of the measured absorption coefficient [35]. Regardless of which variant of the filter-pad technique is used (T, T-R, or IS), a correction for pathlength amplification, commonly referred to as the correction for β-factor, must be applied, and the uncertainties in this correction have been recognized as a major source of error [e.g., 9,24,28,30,32,36,37]. However, establishing an optimal standard protocol for pathlength amplification correction has remained problematic. Most studies dedicated to the determinations of this correction have been made with the T method, and the obtained results for pathlength amplification varied significantly among different studies and sample types. Much of this work is summarized in [30]. Probably the most contentious issue of these studies has to do with the undetermined extent to which the observed differences in pathlength amplification represent artifacts caused by uncertainties in the absorption measurements taken in T configuration using different spectrophotometers with differing measurement geometries as opposed to possible real differences caused by varying sample types and the degree of sample loading on the filters. Reduced differences in pathlength amplification among the sample types and sample loading were observed for the improved T-R and IS filter-pad methods accompanied with improved determinations of true reference absorption on particle suspensions [32,38]. Another issue is that whereas most determinations of pathlength amplification correction in the past were made for the visible spectral range, the correction has often been applied indiscriminately to the ultraviolet (UV) range which may require a different correction [e.g., 31].

A number of factors such as the complexity of light interactions within the sample/filter matrix, different sources of errors in the different filter-pad configurations, and the potential for actual variability in the β-factor associated with variations in the properties of particulate samples and their loading on the filter make it difficult to understand the differences reported in

the literature. This issue highlights the need for further analysis toward consensus recommendations and protocols for filter-pad measurements. In addition, whereas the inside-sphere configuration has long been recognized as a preferred approach to measuring absorption of scattering samples [e.g., 23], very few experiments were dedicated to the determinations of pathlength amplification correction for this configuration of the filter-pad technique. Such determinations for different sample types including natural water and cultures of several phytoplankton species are reported in [32] but more work is needed to test the validity of this approach and to develop a consensus protocol for routine applications of this method.

We have conducted two sets of comprehensive laboratory experiments with various sample types for the purpose of examining the pathlength amplification for the T, T-R, and IS methods of the filter-pad technique and establishing optimal protocols for pathlength amplification correction for applications in routine absorption measurements on arbitrary aquatic samples. One set of experiments included the filter-pad measurements with the T and T-R methods and the other set with the T, T-R, and IS methods. The reference measurements of true absorption of particle suspensions, which are required for the determinations of pathlength amplification, were conducted with two geometrical configurations, i.e., sample outside and inside an integrating sphere. Such reference measurements provide insights into the effects associated with the use of deficient (sample outside the sphere) versus highly accurate (sample inside the sphere) estimates of true absorption on the determinations of pathlength amplification. The uniquely wide scope and comprehensiveness of our experiments also stem from examining a broad range of sample types representing distinctly different particulate assemblages whose size distribution and composition were characterized from ancillary measurements. The examined samples range from phytoplankton cultures and phytoplankton-derived detritus to mineral-dominated samples and natural water samples dominated by inorganic or organic particles including the dominance of phytoplankton. In this paper we describe the results from these experiments and propose the optimal protocols of pathlength amplification correction for the T, T-R, and IS methods. These results also lead to a recommendation of the IS method as the most robust and accurate variant of the filter-pad technique. Our study is focused on the visible spectral range (i.e., light wavelengths in the range from 400 to 700 nm) as the UV range requires a separate dedicated study to address larger variations in pathlength amplification correction observed in this range.

2. OVERVIEW OF MEASUREMENT CONFIGURATIONS AND PATHLENGTH AMPLIFICATION

The original filter-pad technique, which has been most commonly used and recommended as the standard NASA protocol [39], is based on measuring the transmittance (T) of a sample filter relative to a blank reference filter. The filters (the recommended type is glass-fiber filter GF/F) are placed at some distance or just in front of the detector window or at the entrance port to the integrating sphere of the spectrophotometer [Fig. 1(a)]. The T method suffers from a poor geometry of measurement, in which a large fraction of light scattered by the filter is not detected. This results in potentially significant errors in the determination of $a_p(\lambda)$ [27,40]. In the measurement of absorption this error resulting from incomplete collection of scattered light is referred to as the scattering error and is typically corrected with the so-called null-point correction that assumes no true absorption by particles in the NIR. This assumption can be unacceptable, especially for waters rich in absorbing minerogenic particles [40–45]. The T method is also particularly vulnerable to other sources of uncertainties such as variations in filter wetness and filter-to-filter variations in optical properties of filters.

A more advanced approach referred to as the transmittance-reflectance (T-R) method has been proposed to circumvent the limitations associated with the scattering error [26,27]. The T-R method requires multiple spectral scans of the sample and reference filters placed in different positions within the spectrophotometer, specifically at the entrance port (transmittance measurement) and exit port (reflectance measurement) of the integrating sphere [Figs. 1(a) and 1(b)]. The underlying assumptions of the T-R method are based on the law of energy conservation but are not necessarily fully satisfied with the actual geometrical configuration of measurement. The assumptions involved in the calculations and a requirement for multiple scans at different filter positions produce some uncertainties. In addition, the individual filters can occasionally exhibit properties that are significantly different from other filters which can introduce uncertainties difficult to detect and quantify [32]. Despite the demonstrated superiority of the T-R method over the standard T-method [27,32], the T method has been used more commonly than the T-R method. This is probably because the T protocol is considerably simpler, faster, and less laborious than the T-R protocol. In addition, the T-R protocol requires a spectrophotometer equipped with an integrating sphere, which is not needed for the T protocol.

The most advantageous spectrophotometric configuration for measuring particulate absorption which ensures an efficient detection of nearly all photons scattered by the sample and thus minimizes the scattering error to a very low or negligible level involves the placement of the sample inside an integrating sphere [Fig. 1(c)]. The protocol of this inside-sphere (IS) method is fairly simple and no more laborious than the traditional T method. The significant advantages of measuring samples inside an integrating sphere have been demonstrated in experiments with various assemblages of particles in aqueous suspensions [23,32,40,43,44,46,47]. Although rare, the filter-pad technique with the IS configuration has been also used for measuring the particulate absorption on filters [23,32,47,48]. Recently we have also used this method to measure the particulate absorption coefficient of samples that were collected in Arctic waters [33,34]. In addition to the benefit of greatly reducing the scattering error, the filter-pad measurements in the IS configuration are significantly less sensitive to various sources of uncertainties associated with filter scattering properties (such as variations in filter wetness or filter-to-filter differences), and hence these measurements have higher precision and accuracy than measurements with other filter-pad configurations [32]. Although more common use of the IS method

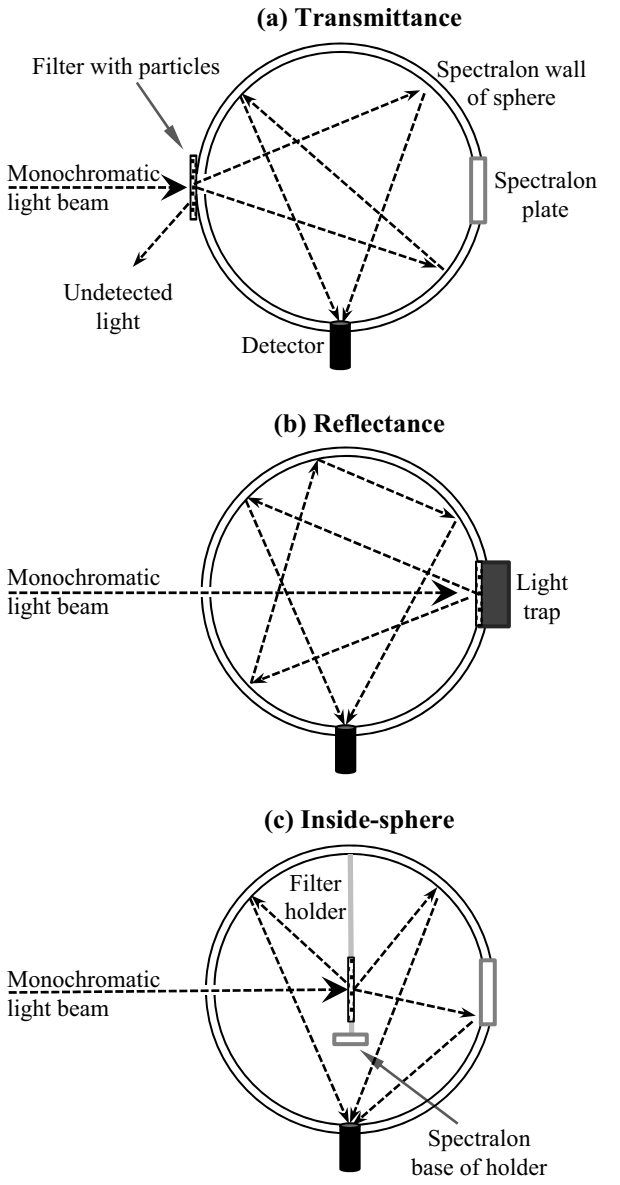

Fig. 1. Generalized schematic illustrating various geometries utilized in the absorption measurement of particles collected on filters. All cases depict the use of an integrating sphere with entrance and exit ports and a detector located at the bottom of the sphere: (a) filter transmittance as measured in both the T and T-R methods; (b) filter reflectance as used in the T-R method; (c) filter placed inside an integrating sphere for the IS method.

in the past was impeded by the requirement for special equipment and accessories (i.e., a relatively large integrating sphere and a fixture for mounting of samples inside the sphere), it is expected that this method will gain widespread use in the near future owing to significant improvements in the accuracy and precision of results.

An important methodological requirement for the application of any variant of the filter-pad technique (T, T-R, or IS) is the use of a predetermined pathlength amplification factor, β. This factor is needed to convert the spectrophotometric data of spectral optical density $OD(\lambda)$ (also referred to as absorbance which is dimensionless) into the absorption coefficient, $a_p(\lambda)$, with physical units (in m^{-1}). The basic formula underlying this conversion for an arbitrary wavelength of light is

$$a_p = \ln(10) OD_f A/(V\beta), \quad (1)$$

where OD_f is the measured optical density of sample filter corrected for baseline (i.e., after subtraction of optical density of blank filter), A the clearance area of the filter (in m^2), and V the filtered volume of the sample (in m^3). Thus the use of appropriate correction for β ensures that the filter-pad technique is quantitative, and as such this method has been also referred in the past to as the quantitative filter technique (QFT) [24].

The pathlength amplification and its practical consequence of enhancement of absorption by pigments as measured in a highly scattering liquid medium was first described by [35]. The β-factor (dimensionless) was defined as a ratio of the actual optical pathlength to the thickness (geometric pathlength) of the sample. Within the context of the filter-pad technique, the enhancement of absorption by particles retained on the filter results from multiple scattering as light propagates through the highly scattering sample/filter matrix. The β-factor is a ratio of the actual optical pathlength within the sample/filter matrix to the geometric pathlength where the latter is defined as V/A. Whereas the optical pathlength is not amenable to measurement, β can be determined as a ratio of OD_f to OD_s on the basis of dedicated experiments, where OD_s is the optical density corresponding to true (reference) absorption of particles within the sample unaffected by the pathlength amplification. It is important to ensure that OD_s is determined from measurements on the particle suspension under the conditions satisfying single scattering regime and is corrected for baseline (i.e., corrected for the optical density of the particle-free medium of the sample). Typically, such measurements are made with a spectrophotometer on relatively dilute particle suspensions contained in a 1 cm cuvette using some geometrical configuration of measurement which may or may not be subject to significant scattering error [e.g., 47] or with a PSICAM instrument with no significant scattering error [32]. Importantly, for the determinations of $\beta(= OD_f/OD_s)$ the measured values of optical density of particles in suspension must be rescaled to the OD_s values that correspond to the geometric pathlength V/A used in the measurement of OD_f. For example, if the measurement on suspension is taken in a 1 cm cuvette and the measurement of OD_f is obtained with $V/A = 10$ cm, the optical density of particles in suspension must be multiplied by 10 to yield OD_s for subsequent determination of β. We note that rescaling of the measurement of OD_f to the geometric pathlength of suspension would be incorrect because OD_f is subject to pathlength amplification that can depend on the particle load on the filter, and hence on the geometric pathlength for the sample filter.

For routine applications of filter-pad technique, instead of using Eq. (1) in which the predetermined values of β are explicit, the most common and recommended approach for correcting the filter-pad measurements for the β-factor is based on the use of a predetermined relationship between OD_s and OD_f [24],

$$OD_s = f(OD_f), \quad (2)$$

where f denotes some function with the input variable OD_f and output variable OD_s. When applying this recommended correction procedure for any given filter-pad sample, the measured OD_f is first converted to OD_s using the predetermined relationship $OD_s = f(OD_f)$, which is then followed by conversion of OD_s to a_p:

$$a_p = \ln(10) OD_s A/V. \quad (3)$$

The key relationship $OD_s = f(OD_f)$ required to correct for pathlength amplification is typically determined from the regression analysis applied to the data of OD_s versus OD_f which are obtained from special laboratory experiments. Note that Eq. (2) does not include an explicit dependence on light wavelength. All spectral data of OD_s and OD_f measured over some selected spectral range of interest (typically the visible part of the spectrum) are considered altogether in these determinations. As the relationship $OD_s = f(OD_f)$ implicitly includes the β-factor, for the sake of convenience we can refer to this relationship and β interchangeably. We note, however, that although the experimentally derived relationship $OD_s = f(OD_f)$ is driven primarily by the pathlength amplification, this relationship and hence the experimental estimates of β are naturally also subject to uncertainties in the measurements of OD_s and OD_f. As discussed above there are several sources of uncertainties and these uncertainties are not generally the same for different geometrical configurations of absorption measurements. The geometrical configuration of measurement itself, which can result in scattering error, has potentially the most important effect on the determinations of OD_s and OD_f. It is therefore important to examine the relationship $OD_s = f(OD_f)$ for different measurement configurations which is one of the focal areas of this study.

The majority of historical data of particulate absorption have been corrected for β-factor that was determined from laboratory experiments in which a poor geometry of measurement (i.e., T-method) was used for both the filter pads and reference measurement on particle suspensions. This could have produced significant scattering errors in these measurements and subsequent error in the determinations of β correction. In addition to the effects of scattering error, the relationship $OD_s = f(OD_f)$ may also vary with optical and physical properties of the sample. Most previous β determinations for the T-method were based on measurements of phytoplankton cultures [e.g., 24,49–52], which is not the most appropriate approach for general applications to natural particulate assemblages containing a variety of particle types. The variations in the literature data of β for the T method are large (more than two-fold) with possible explanations involving various methodological errors and artifacts as well as effects associated with different sample types [e.g., 30].

The determinations of β for the T-R method have been rare compared with the T method but indicated advantages associated with smaller variability in the relationship between OD_s and OD_f [26,38]. The T-R method has not, however, been used widely and routinely for the determinations of particulate absorption in aquatic samples. Most recently, the β determinations were made for the IS method and compared with determinations for the T and T-R methods, which supported the notion that the IS method is superior [32]. In that study the reference measurements of OD_s were made with a PSICAM instrument which reduces the scattering error to a very small or negligible level. The study [32] showed that the β-factor for the IS method is higher than for the T and T-R methods, which is expected from the differences in geometrical configurations of these measurements. The variations in the β-factor for the IS method were observed to be significant (between 3.5 and 5.4) but smaller than the variations for T and T-R method. For the IS method the study [32] proposed to use a constant β-factor of 4.5 for low values of $OD_f (< 0.1)$ and an OD_f-dependent correction for higher OD_f. The proposed formula is, however, discontinuous at $OD_f = 0.1$. Our experiments described below extend the study [32] and other earlier work on pathlength amplification correction toward establishing consensus protocols for the filter-pad technique.

3. METHODS

Two sets of laboratory experiments were conducted with a dual-beam spectrophotometer (Lambda 18, Perkin-Elmer) equipped with a 15-cm Spectralon integrating sphere (RSA-PE-18, Labsphere) with a purpose of examining the pathlength amplification for the three variants, T, T-R, and IS, of the filter-pad technique. The reference measurements on particle suspensions were made in two geometrical configurations (inside and outside the sphere). This experimental design allows us to examine one important source of error in the determinations of pathlength amplification correction for all three filter-pad methods, which is associated with inadequate geometry of reference absorption measurement.

The spectrophotometer was operated in the absorbance mode within the spectral range from 300 to 800 nm in the first set of experiments (referred to as EXPT1) and from 300 to 850 nm in the second set of experiments (EXPT2), providing data of optical density at 1 nm intervals. The spectra were measured with a scan speed of 120 nm/min and a slit of 2 nm. For the filter-pad technique, both the baseline scan for the wet blank filter and the sample scan for the same filter containing particles were measured with an empty (air) reference beam. Prior to the baseline scan, the autozero scan was performed with empty sample and reference beams. The optical density values of blank filters within the visible spectrum varied within the approximate range of 0.4–0.5 and 0.2–0.25 for the T and R measurements, respectively. For the IS measurements, these values were closer to zero, on the order of -10^{-3} to -10^{-2}. For the absorption measurements on particle suspensions, the baseline and sample scans were also made with an empty reference beam. These protocols ensured high quality and reproducibility of measurements.

A. Experiment 1

In the first set of experiments, EXPT1, the filter-pad measurements of OD_f were made in T and T-R configurations. The reference measurements of OD_s of particle suspensions were made in two configurations; one with a 1-cm cuvette mounted inside the integrating sphere and the other with a cuvette placed outside the sphere at the entrance port of the sphere. These absorption measurements were made for a diverse suite of samples which included three mineral-rich samples, two

phytoplankton cultures, two samples dominated by detritus derived from phytoplankton cultures, and three samples of natural seawater with varying contributions of organic and inorganic material (Table 1). All samples were prepared in a way to ensure an appropriate concentration of particles in suspension which yielded sufficiently high signal of OD_s while satisfying the single-scattering condition of measurement. The mineral-rich samples included surface soil dust from Australia (AUS) and Oahu, Hawaii (OAHU) and ice-rafted particles from Kongsfjord, Spitsbergen (SPIT). These samples and their optical properties were described previously [41,44]. The phytoplankton cultures included a centric diatom *Thalassiosira weissflogii* (THAL) and a uniflagellate picoeukaryote *Pelagomonas calceolata* (PELA). Two phytoplankton-derived detrital samples, DETT and DETD, were obtained, respectively, from the cultures of *T. weissflogii* and a green alga *Dunaliella tertiolecta* by exposing the cultures to several freezing/defreezing cycles, ultrasonic treatment, and storing in darkness. The natural seawater samples were collected in Mission Bay (MBAY), a saltwater bay located south of the Pacific Beach community in San Diego (California), and near-shore Pacific waters from the piers in Imperial Beach (IBP1) and Scripps Institution of Oceanography (SIO1) in San Diego. These three samples were optically too thin to allow the measurement of OD_s in a 1-cm cuvette. Therefore, these samples were concentrated by filtering a relatively large volume of the sample (4–12 L depending on the sample) through several polycarbonate membrane filters (0.2 μm, Nuclepore) and resuspending the collected particulate matter in a small volume (~30–70 mL) of seawater. We verified that this procedure of concentrating the particulate matter had a very small effect on the spectral shape of OD_f, which indicates that in a qualitative sense the absorption properties of particulate assemblage did not change significantly. For each sample, two to four different volumes of sample were filtered on the GF/F filters for making T and T-R measurements (Table 1). This approach was undertaken to investigate potential effects of particle loading on the relationship $OD_s = f(OD_f)$.

Table 1. Description of Samples Used in the First Set of β-Experiments (EXPT1)

Sample	Sample Description	Filtration Volumes [mL]
AUST	Surface soil dust from Australia	5, 8, 20, 35
SPIT	Ice-rafted particles from Spitsbergen	5, 10, 15
OAHU	Surface soil dust from Oahu, HI	5, 10, 20, 35
THAL	*Thalassosira weissflogii* culture	5, 10, 20, 35
PELA	*Pelagomonas calceolata* culture	8, 12, 20, 25
DETT	Phytodetritus from *Thalassosira weissflogii*	9, 14, 20, 35
DETD	Phytodetritus from *Dunaliella tertiolecta*	9, 14, 20, 30
MBAY	Seawater from Mission Bay, CA	4, 10, 18, 28
SIO1	Seawater from Scripps Pier, CA	4, 20
IBP1	Seawater from Imperial Beach Pier, CA	4, 10, 20, 30

The standard protocols for the T and T-R filter-pad measurements were used [39,26]. One noteworthy feature of our experimental design is that the measurement of the sample collected on a given filter was preceded by the measurement of baseline for the same filter used as a blank. With this approach, the uncertainties associated with filter-to-filter variability among blank filters were greatly reduced compared with the use of one generic baseline determined by averaging measurements of several blank filters. The latter approach is common in routine applications of the filter-pad technique. In addition, as the measurements were made on freshly prepared samples, potential uncertainties associated with freezing and storage of samples were also avoided. To reduce uncertainties associated with the geometrical configuration of measurements, we applied the so-called null-point correction to the measurements of OD_f in both T and T-R configurations. This correction assumes no particle absorption in the near-infrared (NIR) spectral region, typically at wavelengths of about 750 nm or longer. With this correction, the spectral values of optical density are shifted across the examined spectrum to satisfy this assumption in the NIR. The null-point correction is a typical procedure for the T method because these measurements are known to be subject to scattering error and other artifacts resulting in a potentially significant shift of the measured signal, which is unrelated to actual particulate absorption. In EXPT1, the uncorrected OD_f values in the NIR obtained with the T method ranged from slightly negative values (on the order of -10^{-3}) for phytoplankton cultures to positive values exceeding 0.055 for mineral-rich samples. For the T-R method, the range of uncorrected OD_f in the NIR was somewhat smaller, from negative values on the order of -10^{-3} to about 0.04, the latter being one order of magnitude below the measured values in the blue spectral region. Although the T-R method was originally designed to avoid the necessity for null-point correction [26,27], we found it reasonable to apply this correction to our T-R data from EXPT1. This was done for consistency with results obtained from reference measurements on particle suspensions as described below, and also because the T-R measurements can still include some shift of the measured signal which is unrelated to actual absorption by particles.

The reference measurements of OD_s were made on optically thin particle suspensions contained in a 1-cm cuvette, which ensured that the multiple scattering effects were negligible [e.g., 53,54]. For baseline measurements, the filtered medium of the sample (i.e., seawater or culture medium filtered through a 0.2 μm Millipore filter) was used. Typically, an average of two to four replicate scans of sample and two replicate scans of baseline were used for determining the final data of OD_s. The reproducibility of replicate measurements was very good, typically within a few percent.

The measurements of OD_s inside the integrating sphere provide the best possible reference estimate of true absorption. The measurement uncertainties are very small because this configuration reduces the scattering error to a very small or negligible level [23,40,47]. For clarity, we choose not to use the acronym IS in the context of measurements on particle suspensions inside the integrating sphere as this acronym is used exclusively in the context of filter-pad technique. The use of

reference measurements inside the integrating sphere represents the key advancement in the experimental design for determining the pathlength amplification compared with most similar determinations in the past. Details of our methodology for measuring absorption of particle suspensions inside the integrating sphere are described elsewhere [41,43,44,47]. One minor methodological artifact described and explained in those studies which deserves attention is that the measured signal in the NIR is slightly negative for particles that do not absorb in this spectral region or have very small absorption close to the limit of detection. For all samples examined in EXPT1, the measured OD_s in the NIR was slightly negative, ranging from about −0.003 for the phytoplankton culture of *P. calceolata* to about −0.0001 for the MBAY sample. Whereas we recognize the possibility that a few samples, such as that from Mission Bay, could have had a small NIR absorption (at least one order of magnitude lower than in the blue), we applied a null-point correction consistently to the OD_s spectra of all samples to eliminate this minor negative offset. Because the T and T-R filter-pad methods cannot accurately quantify the potential presence of very small absorption in the NIR and the main purpose of EXPT1 was to determine the relationship $OD_s = f(OD_f)$ within the visible spectral region (400–700 nm) for these two filter-pad methods, the application of a consistent null-point correction procedure to both the reference measurements on suspensions and the filter-pad measurements with T and T-R methods is reasonable and justifiable.

Measurements of OD_s of particle suspensions in a cuvette placed outside the integrating sphere were also made. These measurements can naturally be subject to significant scattering error [47] so we also applied the null-point correction to these measurements. The NIR offset in OD_s measured with the cuvette outside the sphere was positive for all samples, extending to values as high as 0.02 for mineral-rich samples. We note that such deficient geometry of reference measurements has been used for almost all historical determinations of β-factor for the T method of filter-pad technique. The main value of including both the optimal and poor geometric configuration of reference measurement of OD_s in our experiments is to demonstrate the effect of inadequate reference measurements on β determinations. We also note that all final spectra of OD_s and OD_f in EXPT1 were smoothed multiple times with a five-point (i.e., 5-nm) moving average to smooth out small-scale irregularities in the spectra associated with instrument noise.

Summarizing EXPT1, the different measurement configurations, the range of different types of samples, and multiple volumes of samples examined in this experiment provided a comprehensive dataset in support of the development of consensus protocol for pathlength amplification correction for the T and T-R methods. With the two configurations of the reference measurements on particle suspensions and the two configurations of the filter-pad technique, EXPT1 allowed us to determine the relationship of $OD_s = f(OD_f)$ for the four specific experimental settings, i.e., T with a reference suspension inside sphere, T with a suspension outside sphere, T-R with a suspension inside sphere, and T-R with a suspension outside sphere.

B. Experiment 2

The primary goal of the second set of experiments, EXPT2, was to examine the pathlength amplification for the optimal inside-sphere configuration of the filter-pad technique. For the IS filter-pad measurements, the filter was mounted in a custom-built fixture similar to the cuvette holder used for inside-sphere measurements of liquid samples. The illuminated portion of the filter has no contact with solid surface. The measurements of reference absorption of particle suspensions were made using the same optimal geometric configuration with a cuvette inside the sphere. The additional measurements on suspensions in a cuvette placed outside the sphere and the filter-pad measurements in the T and T-R configurations were also made in EXPT2.

Six different types of samples were examined including four natural seawater samples, a sample derived from Arctic sea ice, and a sample containing a mixture of four phytoplankton cultures (a small green algae from the genus *Nannochloropsis*, a green alga *Chlorella vulgaris*, a centric diatom *Thalassiosira pseudonana*, and a red alga *Porhyridium cruentum*) (Table 2). The Arctic sea ice sample was collected during the NASA ICESCAPE cruise in the Chukchi Sea [55] and exhibited large concentration of particulate matter within ice. By thawing a piece of ice we obtained a particulate suspension dominated by minerogenic particles. Three samples of natural seawater were collected in near-shore waters of San Diego from the piers in Imperial Beach (IBP2) and Scripps Institution of Oceanography (SIO2 and REDT). The REDT was collected during a red tide formed by the dinoflagellate *Lingulodinium polyedrum*. One additional sample was collected at an offshore location from San Diego (OCEA). Similar to EXPT1, all four samples of natural seawater were concentrated by filtration of relatively large volume of seawater on several 0.2 μm polycarbonate membrane filters and subsequent resuspension of retained particulate matter in a small volume of seawater. For all but one sample, multiple volumes were measured with the IS method (Table 2). The T and T-R measurements were made only for one sample volume. This approach was employed in

Table 2. Description of Samples Used in the Second Set of β-Experiments (EXPT2)

		Filtration Volumes [mL]	
Sample	Sample Description	IS Method	T, T-R Method
ARCT	Particles from melted Arctic sea-ice	9, 19, 41	41, 41
PHYT	Mixture of four phytoplankton cultures	3, 9, 15	n/a[a], n/a
REDT	Red tide from Scripps Pier (*L. polyedrum*)	3, 7, 15, 23	15, n/a
SIO2	Seawater from Scripps Pier	5	5, 5
OCEA	Seawater from offshore San Diego	9, 14.5	14.5, 14.5
IBP2	Seawater from Imperial Beach Pier	5, 10, 17, 25	25, 25

[a]"n/a" refers to not applicable as the measurement was not performed.

EXPT2 because our focus was on the IS method and more extensive measurements with the T and T-R methods were made in EXPT1. In addition, the practicality of making so many different measurements nearly in parallel is highly limited.

The protocols for the acquisition and processing of absorption data were generally similar to those used in EXPT1 with some differences in the details. The main difference is with regard to the null-point correction in the NIR. In EXPT2, no null-point correction was applied to reference measurements on sample suspensions and sample filters placed inside the sphere. For some samples, these measurements showed significant absorption in the NIR. In principle, the T-R configuration of the filter-pad technique does not require the null-point correction, so these measurements were not corrected either. In EXPT2, the null-point correction was applied only to the measurements on sample suspensions outside the sphere and T measurements on filters. For measurements of OD_s inside the sphere replicate spectral scans were taken and averaged. The number of replicates depended on the sample, ranging from two scans for the PHYT sample to 10 scans for IBP2. The larger number of replicates was taken when the measured signal was relatively low with higher contribution of instrument noise. For the sample suspensions outside the sphere, two to three replicates were taken. For the IS measurements of OD_f on filters, two replicate scans were measured and averaged for each sample (the filters were rotated by about 90° for the replicate measurement, thus exposing a somewhat different portion of the sample to the illuminating beam of light). The reproducibility of replicate measurements was very good in all cases, typically within a few percent. No replicate scans were made for OD_f measurements in T and T-R configurations. For each sample filter, the baseline was obtained with the same filter used as a blank. The smoothing procedure was optimized for each spectrum individually depending on the general spectral shape, its main features such as the presence of strong absorption maxima associated with phytoplankton pigments, and the presence of instrument noise. In general, when phytoplankton absorption maxima were present, smoothing within these spectral bands was made with a three-point (3-nm) moving average. Outside these spectral bands and for the spectra with no phytoplankton features the data were smoothed with a five-point or nine-point moving average.

In addition to absorption measurements, in EXPT2 we made ancillary measurements to obtain a more comprehensive characterization of optical properties of examined particles and also their size distribution and composition. Specifically, we measured the spectra of the beam attenuation coefficient of particles in suspension, $c_p(\lambda)$, with a Perkin-Elmer spectrophotometer using a special geometrical configuration of measurement [e.g., 44]. These measurements, in conjunction with the determination of the absorption coefficient of particles, $a_p(\lambda)$, from the measurement of $OD_s(\lambda)$ inside the sphere, provide the spectra of particulate scattering coefficient, $b_p(\lambda)[= c_p(\lambda) - a_p(\lambda)]$, and an additional optical property of the single-scattering albedo, $\omega_{op}(\lambda)[= b_p(\lambda)/c_p(\lambda)]$. We calculated the spectral slope, γ, of the scattering coefficient by fitting a power function to the measured spectra over the wavelength range from 300 to 850 nm.

The concentrations of dry mass of suspended particulate matter (SPM), particulate organic carbon (POC), and chlorophyll-*a* (Chla) were also determined. For samples IBP2, SIO2, REDT, and OCEA, these determinations were made on original seawater samples, and not on the concentrated samples used for pathlength amplification absorption measurements. This is because the available volume of concentrated samples was not sufficient to carry out these ancillary measurements. For PHYT and ARCT, however, the SPM, POC, and Chla determinations were made for the same samples as the absorption measurements. A standard gravimetric method for SPM and a high temperature combustion method for POC determinations were used [e.g., 56,57]. Details of protocols used in our experiments are described in [58,59]. For all samples with the exception of the culture mix, duplicate determinations of SPM and POC were made and averaged. The mean values for SPM and POC agreed with the individual measurements to within ~15% and 6%, respectively. Chla was determined with a spectrophotometric method in 90% acetone extracts of the samples [60]. A quadrichroic equation involving the optical density of extracts measured in 1-cm cuvette at light wavelengths of 630, 647, 664, and 691 nm was used. These measurements were made with a cuvette placed inside the integrating sphere of the Perkin-Elmer Lambda 18 spectrophotometer. No Chla determinations were made for the sample derived from the Arctic sea ice as the pigment level was undetectable. The determinations of SPM, POC, and Chla provide proxies for particulate composition in terms of contribution of organic (or inorganic) particles to total particulate matter (POC/SPM) and a contribution of phytoplankton to total particulate matter (Chla/SPM).

The particle size distribution (PSD) of the samples (with the exception of SIO2) was measured with a Coulter technique (Beckman-Coulter Multisizer III) using both 30- and 200-μm aperture tubes, thus covering the size range from about 0.7 to 120 μm [61]. Measurements of the PSD were made on the concentrated sample used for optical measurements, with typically 15–25 replicate measurements obtained and averaged for each aperture and merged into a single distribution.

4. RESULTS AND DISCUSSION

A. Optical and Particle Properties of Samples

The samples examined in EXPT1 and EXPT2 exhibit a broad range of variability in the spectral shape of light absorption (Fig. 2). This figure illustrates the spectra of $OD_s(\lambda)$ measured on particle suspensions inside the integrating sphere, which represent the best reference measurements of particle absorption used in the determinations of the pathlength amplification relationship $OD_s = f(OD_f)$ as described later. The $OD_s(\lambda)$ values for the AUS, SPIT, and OAHU samples from EXPT1 show a decrease with increasing light wavelength, which is characteristic of particle assemblages dominated by minerals. An earlier study [44] indicated that these samples have a very low ratio of POC/SPM (less than 0.04), which is indicative of the dominance of inorganic material. For such assemblages, the spectral shape of absorption can exhibit considerable changes in the spectral slope within the visible part of the spectrum and depart significantly from an exponential curve that is often used to

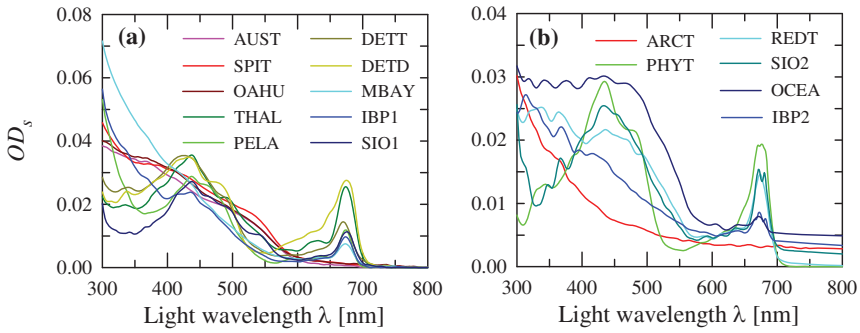

Fig. 2. Example spectra of optical density for particle suspensions, OD_s, measured inside an integrating sphere for the two sets of experiments: (a) EXPT1; (b) EXPT2. Descriptions of sample names for individual spectra are provided in Tables 1 and 2.

approximate the absorption spectra of organic-dominated nonalgal particulate matter. Phytoplankton spectra in EXPT1 are represented by samples of single species cultures, THAL and PELA. These species have different pigment composition and cell size which result in differences in the shape of absorption spectra. For the two phytoplankton-derived detrital samples, DETT and DETD, the absorption spectra are actually different from a typical exponential-like featureless spectrum of organic detritus. The DETT and DETD spectra show distinct blue and red maxima associated with algal pigments, but the position of the peaks is shifted somewhat to shorter wavelengths compared with the position observed for healthy phytoplankton cells. This shift is characteristic of degraded pigments. Another feature of pigment degradation is a nearly twofold decrease in the magnitude of the red maximum, which is evident by comparing the results for DETT and THAL, both representing the culture of *T. weissflogii*. This decrease is consistent with a ratio of the molar-specific absorption coefficients of degraded pigments and chlorophyll-*a*, which is 0.56 in the red spectral band in the acetone solvent [62].

Significant differences are also observed in the spectral shape of $OD_s(\lambda)$ among the three natural seawater samples examined in EXPT1. The MBAY sample from Mission Bay is most likely dominated by organic detritus with a relatively small contribution of phytoplankton as indicated by featureless increase of absorption with decreasing wavelength throughout most of the visible spectrum into the UV and a relatively small absorption maximum associated with chlorophyll-*a* in the red. The nearshore samples, IBP1 and SIO1, appear to have a higher proportion of phytoplankton because the absorption maximum in the blue is clearly noticeable.

The absorption spectra also differ greatly among the samples examined in EXPT2. In addition to PHYT, two samples of natural seawater, REDT and SIO2, show well-pronounced phytoplankton absorption maxima in the blue and red spectral bands. In contrast, the ARCT sample derived from sea ice shows a featureless spectrum with a decrease in absorption magnitude with increasing wavelength. The IBP2 and OCEA samples are characterized by intermediate shapes of absorption spectra, indicating a relatively large contribution of nonalgal particles and lower contribution of phytoplankton. Interestingly, these two samples and also the ARCT and SIO2 samples show significant absorption in the NIR spectral region. This suggests the presence of certain types of nonalgal, most likely minerogenic, particles that have high efficiency of absorption in the NIR. In contrast, the phytoplankton sample (PHYT) and the REDT sample representing the bloom of dinoflagellate *Lingulodinium polyedrum* have essentially no or undetectable absorption in the NIR.

The patterns and differences in the absorption spectra among the samples of EXPT2 are consistent with data characterizing the composition of particulate matter in the samples (Table 3). The examined samples cover a broad range of POC/SPM from 0.04 to 0.44, which reflects large differences in the proportion of organic and mineral particles. As expected, whereas the PHYT and REDT samples are characterized by the highest values of POC/SPM indicating the dominance of organic material, more specifically phytoplankton in these two cases, the mineral-dominated ARCT sample has the lowest POC/SPM. The IBP1, SIO2, and OCEA samples are intermediate with a mixed, more balanced organic/inorganic composition of particulate matter, although SIO2 and OCEA have clearly a higher fraction of organics than IBP2. The range of Chla/SPM and POC/Chla ratios is also very large and spans more than one order of magnitude, and even more considering that the ARCT sample has undetectable levels of Chla (Table 3).

In addition to large variation in particle composition, the samples also differ significantly in terms of particle size distribution (Fig. 3). For example, the red-tide sample REDT shows a distinct maximum between 30 and 40 μm associated with a high abundance of large cells of the bloom forming species of *Lingulodinium polyedrum*. This sample has also the largest contribution of small submicrometer particles. As a result of these distinct features associated with both very small and large particles, the REDT has the lowest value for the median diameter, $D_v^{50} = 0.95$ μm, and the highest value for the 90th percentile diameter, $D_v^{90} = 31.5$ μm, as derived from the particle volume size distribution (Table 3). The OCEA and IBP2 samples also show substantial abundance of submicrometer particles. However, the IBP2 additionally has the largest proportion of particles within the size range from a few micrometers to about 15 μm, so this sample has the second largest value of $D_v^{90} = 10.2$ μm (Table 3). The size distribution of PHYT shows features associated with the mix of phytoplankton species in the sample. Two peaks within the size range from approximately 1

Table 3. Indicators of Particle Composition, Size, and Optical Characteristics for the Samples Used in EXPT2[a]

	Indicator	Units	ARCT	PHYT	REDT	SIO2	OCEA	IBP2
Composition	POC/SPM	dim	0.04	0.44	0.37	0.20	0.23	0.12
	Chla/SPM	dim	n/d	7.3×10^{-3}	1.6×10^{-3}	2.3×10^{-3}	2.7×10^{-4}	9.3×10^{-4}
	POC/Chla	dim	n/d	61	235	88	860	127
Size	D_v^{50}	μm	2.19	1.72	0.95	n/d	1.19	2.51
	D_v^{10}	μm	0.84	0.94	0.73	n/d	0.74	0.79
	D_v^{90}	μm	7.35	6.25	31.5	n/d	6.40	10.2
Optical	$\omega_{op}(440)$	dim	0.96	0.83	0.90	0.87	0.87	0.92
	$\omega_{op}(660)$	dim	0.98	0.88	0.95	0.94	0.96	0.96
	γ	dim	−0.59	−0.89	−0.25	−1.03	−0.78	−0.80

[a]For natural seawater samples (REDT, SIO2, OCEA, IBP2), the compositional indicators represent the original sample before concentration. Size and optical indicators all pertain to the concentrated sample used for experiments. D_v^{50} represents the median particle diameter derived from the particle volume distribution over the size range 0.7–120 μm, with values for the 10th and 90th percentile also reported. ω_{op} is the value of the particle single-scattering albedo at the two indicated light wavelengths. The spectral dependence of the particle scattering coefficient, γ, is calculated over the wavelength interval 300–850 nm. "n/d" refers to not determined, and "dim" to dimensionless.

to 2 μm are associated with *Nannochloropsis*. The presence of these two peaks was also observed in the culture of *Nannochloropsis* before the mixed sample was prepared. The PHYT sample also shows distinct features in the size ranges of 5–5.5 μm and 8–9 μm, which are associated with *T. pseudonana* and *P. cruentum*, respectively. A small feature of *C. vulgaris* between approximately 2.5 and 3 μm, although much less pronounced compared with the features of the three other species, can also be seen in the size distribution of PHYT. Because PHYT has the lowest contribution of relatively large particles above 10 μm, this sample has the lowest value of $D_v^{90} = 6.25$ μm among the examined samples (Table 3).

The highly diverse nature of samples is further supported by the variability in the optical properties presented in Fig. 4 and Table 3. The spectral slope (γ) of the particle scattering coefficient, $b_p(\lambda)$, is steepest for the SIO2 sample ($\gamma = -1.03$) [Fig. 4(a)]. Steepening of the slope of $b_p(\lambda)$ spectrum is typically caused by an increasing proportion of small-sized particles [63]. The particle-size distribution was not measured for the

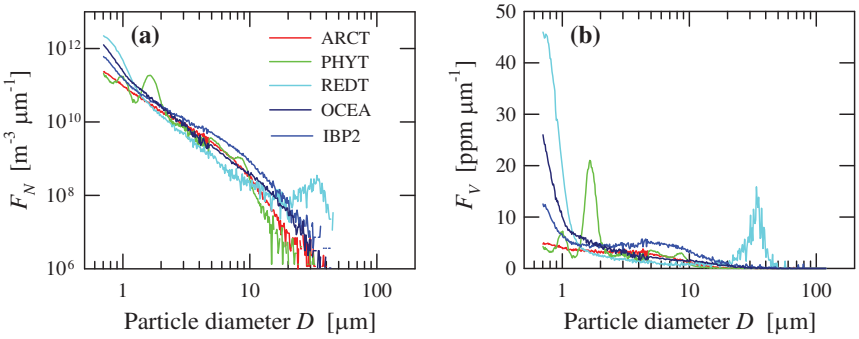

Fig. 3. Particle size distributions measured on the concentrated samples used in EXPT2: (a) density functions of particle number concentration, F_N; (b) density functions of particle volume concentration, F_V, as a function of equivalent spherical diameter D.

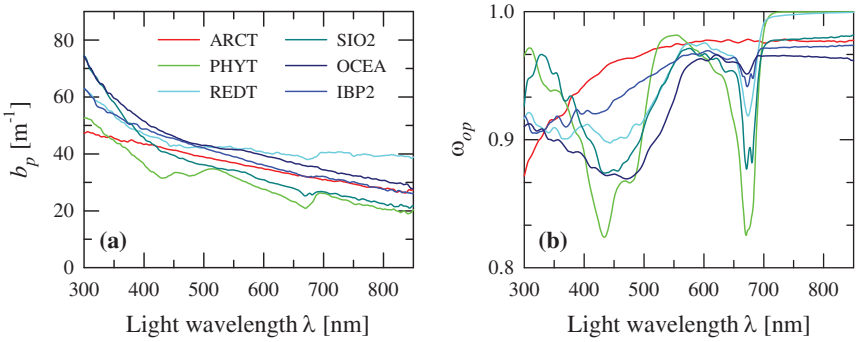

Fig. 4. Optical properties of the particle assemblages used in EXPT2. Depicted are spectra of: (a) the particle scattering coefficient, b_p; (b) the single-scattering albedo of particles, ω_{op}.

SIO2 sample, but this cause and effect pattern is consistent with our data for the remaining five samples from EXPT2. For example, the flattest spectrum of $b_p(\lambda)$ was measured for the REDT sample ($\gamma = -0.25$), which has the highest proportion of large particles as indicated by the largest value of D_v^{90} (Table 3). In contrast, the scattering slope of PHYT is very steep ($\gamma = -0.89$), and this sample has the smallest value of D_v^{90}.

The variations in the relative roles of absorption and scattering processes in the attenuation of a light beam by different samples are demonstrated in terms of the single scattering albedo of particles, $\omega_{op}(\lambda)$ [Fig. 4(b)]. Concomitant with an increase in $\omega_{op}(\lambda)$ is an increase in the role of scattering and a decrease in the role of absorption. Within the visible part of the spectrum, the extreme spectra of $\omega_{op}(\lambda)$ correspond to the PHYT and ARCT samples. Whereas in the blue and red bands of maximum absorption by phytoplankton the PHYT sample has the values of $\omega_{op}(\lambda)$ as low as approximately 0.82, the corresponding values for ARCT exceed 0.95. Note also that in the green waveband of minimum absorption by phytoplankton, PHYT has the highest value of $\omega_{op}(\lambda)$ (slightly above 0.98 at $\lambda = 550$ nm) among the examined samples. This result is consistent with the expectation that phytoplankton have the largest range of $\omega_{op}(\lambda)$ within the visible spectral range.

B. Pathlength Amplification Correction

As pointed out earlier, the recommended approach for correcting the filter-pad measurements for pathlength amplification involves the use of the relationship $OD_s = f(OD_f)$ followed by the calculation of absorption coefficient from Eq. (3). This section is focused on main results from our experiments, specifically the relationship $OD_s = f(OD_f)$. Figures 5 and 6 depict example data of OD_s versus OD_f for each sample examined in EXPT1 and EXPT2, respectively. The presented data cover a broad spectral range from 300 to 800 nm with the lowest values of OD_f corresponding to the NIR and the highest values generally within the UV. For EXPT1, we present the data of OD_s obtained from measurements on particle suspension inside the integrating sphere as a function of OD_f obtained with the T-R method of filter-pad technique (Fig. 5). This figure includes four panels, each depicting data for two or three samples representing the same general category of samples, namely mineral-dominated, natural water, phytoplankton cultures, and phytoplankton-derived detrital samples. For the three mineral-dominated samples, AUST, SPIT, and OAHU, the OD_s versus OD_f curves are similar to one another and display a regular trend over the entire examined range of OD_f and hence the entire spectral range including the UV [Fig. 5(a)]. In contrast, for other categories of samples, the differences in the OD_s versus OD_f relationships among the samples are large in the UV spectral region, and in some cases are also significant in the blue spectral region. For example, the relationships for the three natural water samples, MBAY, IBP1, and SIO1, diverge considerably at OD_f values larger than approximately 0.15, which correspond to the UV

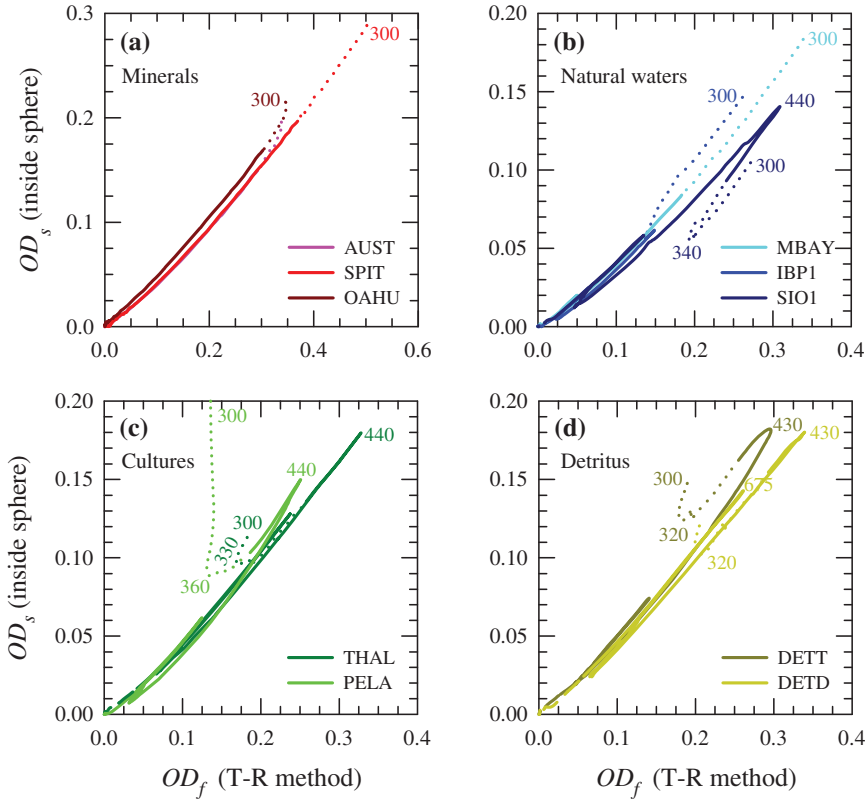

Fig. 5. Example relationships between optical density of particle suspension, OD_s, measured within an integrating sphere and measured optical density of sample filter, OD_f, determined using the T-R method over the spectral range 300–800 nm for the samples in EXPT1. The four panels represent individual broad categories of samples as indicated. For each spectrum, the UV region is displayed as a dotted line, the VIS region as a solid line, and the NIR as a dashed line. Measurements at 300 nm and for regions of strong spectral curvature or hysteresis are labeled in each panel.

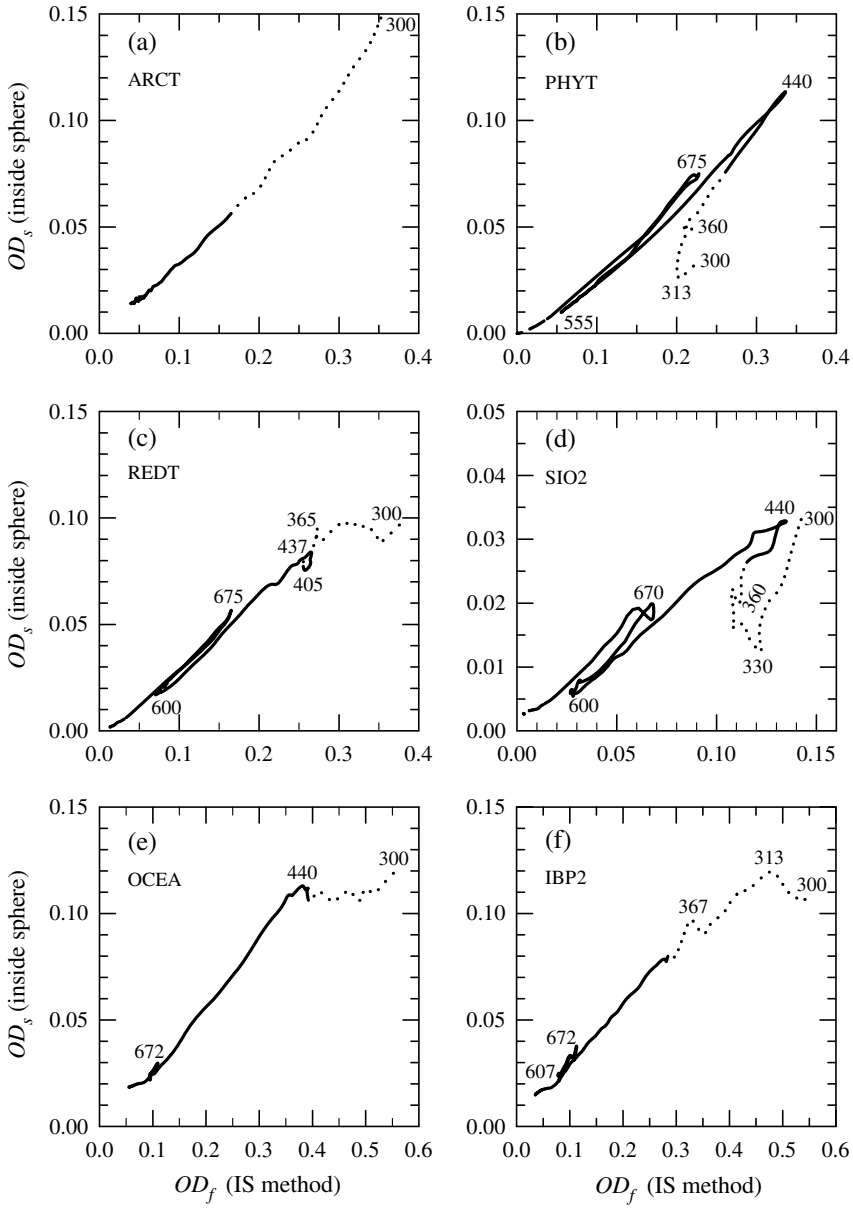

Fig. 6. Similar to Fig. 5, but for EXPT2 samples with OD_f measured inside the integrating sphere.

spectral range and to some extent also the short-wavelength portion of the visible spectrum [Fig. 5(b)]. In addition, the SIO1 sample whose absorption spectrum is dominated by phytoplankton [Fig. 4(a)] exhibits the so-called "hysteresis-like" patterns within the blue and red wavebands of phytoplankton absorption maxima [Fig. 5(b)]. The hysteresis pattern indicates that OD_s assumes different values for the same value of OD_f measured at different wavelengths located on the ascending and descending sides of the absorption maximum. Such hysteresis patterns and divergence of relationships in the UV are also observed for the phytoplankton cultures [Fig. 5(c)] and phytoplankton-derived detrital samples [Fig. 5(d)].

The example data of OD_s versus OD_f from EXPT2 presented in Fig. 6 were determined using the optimal configuration of measurements for both OD_s and OD_f with the particle suspensions and filter pad samples placed inside the integrating sphere. For all samples except for ARCT, the relationship OD_s versus OD_f shows significant departure in the UV from a well-behaved regular trend within the visible spectral region. We recall that the ARCT sample is dominated by mineral particles exhibiting a fairly featureless increase of absorption with decreasing wavelength over the entire examined spectral range [Fig. 4(b)]. The result that the mineral-dominated ARCT sample with a featureless absorption spectrum shows a regular trend of OD_s versus OD_f over the entire spectral range including the UV [Fig. 6(a)] is consistent with results from EXPT1 [Fig. 5(a)]. Three samples from EXPT2, PHYT, REDT, and SIO2, show the hysteresis patterns within the visible spectral region [Figs. 6(b), 6(c), and 6(d)]. The dominant features of the absorption spectra of these three samples are the blue and red maxima associated with phytoplankton [Fig. 4(b)] so the presence of hysteresis for these samples is consistent with results

for phytoplankton-dominated samples from EXPT1, i.e., SIO1, THAL, PELA, DETT, and DETD. Note also that the samples IBP2 and OCEA from EXPT2 lack or have less-pronounced hysteresis patterns in the [Figs. 6(e)–6(f)], which can be attributed to the lack of dominant maxima in absorption spectra [Fig. 4(b)]. In contrast to ARCT, however, these two samples show a clear deviation in the behavior of OD_s versus OD_f in the UV from a regular trend within the visible part of the spectrum.

The results presented in Figs. 5 and 6 indicate that the behavior of the OD_s versus OD_f relationship in the UV can be highly variable and inconsistent among different samples, which implies that it is difficult to predict with a generalized formula. These results also caution against indiscriminate use of pathlength amplification correction in the UV spectral range with the relationship developed for the visible range. The challenges in obtaining quantitatively robust and accurate results in the UV from the filter-pad technique associated, for example, with the instability of UV-absorbing compounds during the handling and filtration of samples were also recognized in past studies [31]. Clearly, further studies dedicated specifically to the UV spectral range are needed. In the following presentation of the OD_s versus OD_f relationships, the analysis of our data from EXPT1 and EXPT2 is restricted to the visible spectral range from 400 to 700 nm.

As shown above, the hysteresis patterns may compromise, to some extent, the OD_s versus OD_f relationships within the visible spectral region. Such patterns were also observed in previous studies [9,31,32,36,38,51]. Several possible sources for the presence of these patterns were suggested, including the methodological errors in measurements of OD_s and OD_f [28] and artifacts during the handling and filtration of samples such as the loss of water-soluble pigments [32]. Note that if the hysteresis patterns were real and not just a result of some methodological artifact, it would indicate that the OD_s versus OD_f relationship exhibits some dependence on light wavelength. We have no evidence that some methodological artifacts could have produced the hysteresis patterns in our data. In fact, an important role of artifacts seems unlikely because while using the same optimal measurement configuration with inside-sphere samples for determining both OD_s and OD_f we observed the hysteresis patterns for some samples, but not all samples. Without further speculation on possible sources of hysteresis observed in our data, it is important to re-emphasize that these patterns are well-pronounced in the samples that exhibit distinct absorption maxima in the blue and red wavebands produced by phytoplankton pigments. Although the hysteresis patterns introduce some variability in the OD_s versus OD_f relationships, the presence of this variability has been tolerated in the typical approach in which this relationship is examined

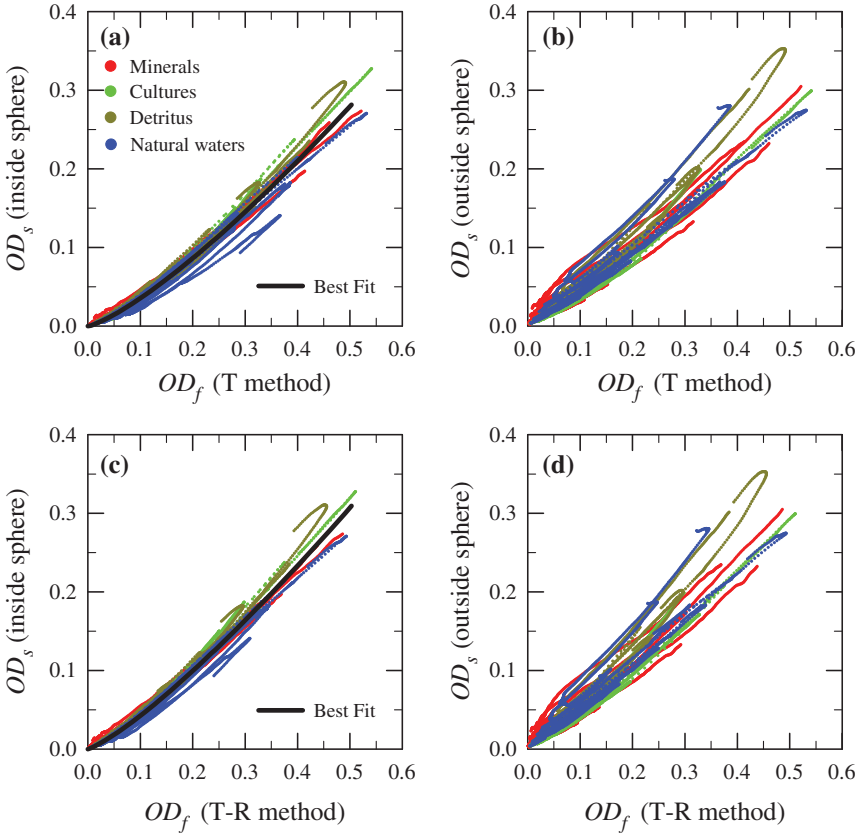

Fig. 7. Relationships between OD_s and OD_f obtained for EXPT1 samples using two configurations for the measurement of OD_f, the T method [(a), (b)] and the T-R method [(c), (d)], and two configurations for the measurement of OD_s, with the suspension cuvette placed either inside [(a), (c)] or outside of [(b), (d)] the integrating sphere. The symbol legend provided in panel (a) is applicable to all four panels. For panels (a) and (b), the best fit of a power function to the data is also indicated (Table 4).

without regard to light wavelength. This wavelength-independent approach is also used in our analysis presented below.

Figure 7 depicts the OD_s versus OD_f relationships based on data collected in EXPT1 for the T and T-R methods of the filer-pad technique. For each method, the results are presented for two configurations of OD_s measurements, i.e., the particle suspensions placed inside the integrating sphere and outside the sphere. The presented data are from the 400–700 nm spectral range, and the different categories of samples examined in EXPT1 are shown in different colors. The main goal of examining such data is to establish the best fitting function representing the relationship of OD_s versus OD_f (Eq. (2)] for subsequent use in the pathlength amplification correction. Smaller scatter in the data points of OD_s versus OD_f implies smaller uncertainties in pathlength amplification correction. The data points exhibit generally considerable scatter between the examined samples for the four methodological scenarios presented in Fig. 7. However, there are also significant differences in the extent of this scatter between the scenarios. Specifically, there is a much smaller scatter in data points for OD_s measurements made on particle suspensions placed inside the integrating sphere compared with the outside-sphere measurements. This result is well-pronounced regardless of whether OD_f was measured with the T method [Figs. 7(a) and 7(b)] or T-R method [Figs. 7(c) and 7(d)]. For example, for the OD_f value of 0.2 obtained with the T method, the range of OD_s expressed as a ratio of maximum to minimum value is 1.69 for the inside-sphere and 1.82 for the outside-sphere measurements. For the same OD_f but obtained with the T-R method, the respective ratios are 1.41 and 1.86.

These results highlight the critical importance of making the reference measurements on particle suspensions with the best possible geometric configuration such as our inside-sphere configuration and attest to potentially severe limitations in most historical determinations of OD_s versus OD_f relationships, which were developed for the T method using a poor geometrical configuration of measurements on particle suspensions, more or less similar to our outside-sphere configuration. Note also that the scatter in data points of OD_s versus OD_f can be reduced if OD_f measurements are made with the T-R method as compared with the T method. This result is evident for the inside-sphere configuration of OD_s measurements [Figs. 7(a) and 7(c)] but not clearly discernible when OD_s was measured with the inferior outside-sphere configuration [Figs. 7(b) and 7(d)]. Because it is the inside-sphere measurement that provides the best determinations of OD_s, our results support a generalized conclusion that the T-R method is superior to the T method in terms of producing more robust relationship between OD_s and OD_f. This conclusion is consistent with findings in previous studies [27,32,38].

The data in Figs. 7(a) and 7(c) provide a basis for establishing the best fitting functions $OD_s = f(OD_f)$ for the T and T-R methods, respectively. The quadratic function of the form $OD_s = C_1 OD_f + C_2 OD_f^2$, where C_1 and C_2 are the best fit coefficients determined from the regression analysis, was used in most previous studies [e.g., 24,26,49–52,64–66]. The use of a power function $OD_s = k\, OD_f^{\kappa}$, where the best fit coefficients are denoted by k and κ, was also shown to provide an adequate approach in the study of [9]. By applying nonlinear regression analysis (a standard Levenberg–Marquardt algorithm built into MATLAB software package, *MathWorks*) we examined both types of functions for fitting the data in Figs. 7(a) and 7(c). The fitted functions and the statistical parameters characterizing the goodness of fit are presented in Table 4. The fit with the power function is slightly better than the quadratic function so our recommendation with regard to pathlength amplification correction of the filter-pad measurements with the T and T-R methods is to use the power functions. These functions are also plotted in Figs. 7(a) and 7(c). We note that these functions were calculated for the range of OD_f extending to about 0.5 but in practice it is most desirable to work within the range below 0.4.

Figure 8 depicts the OD_s versus OD_f relationships for data within the visible spectral range obtained with different methodological scenarios in EXPT2. These data re-emphasize the shortcomings of measuring OD_s outside the integrating sphere and clearly demonstrate that the use of optimal inside-sphere measurements of OD_s results in higher quality of relationships between OD_s and OD_f for all three methods of the filter-pad technique, T [Figs. 8(a) and 8(b)], T-R [Figs. 8(c) and 8(d)], and IS [Figs. 8(e) and 8(f)]. In particular, whereas the variations

Table 4. Fitted Functions and Goodness-of-Fit Statistics for the Relationship between Optical Density Measured on Suspensions (OD_s) and on Glass-Fiber Filters (OD_f)[a]

Method and Function	R^2	RMSE	MNB (%)	NRMS (%)	N
T method					
$OD_s = 0.679\ OD_f^{1.2804}$	0.982	0.00826	−2.38	19.46	11137
$OD_s = 0.322\ OD_f + 0.506\ OD_f^2$	0.981	0.00847	10.89	24.42	11137
T-R method					
$OD_s = 0.719\ OD_f^{1.2287}$	0.988	0.00682	−2.71	18.56	11137
$OD_s = 0.388\ OD_f + 0.496\ OD_f^2$	0.987	0.00710	9.23	21.86	11137
IS method					
$OD_s = 0.323\ OD_f^{1.0867}$	0.985	0.00351	1.44	12.09	5117
$OD_s = 0.256\ OD_f + 0.111\ OD_f^2$	0.985	0.00358	4.32	13.25	5117

[a]Data from EXPT1 were used for fitting equations and computing statistics for the T and T-R methods, and data from EXPT2 were used for the IS method. Measurements of OD_s were all obtained with the particle suspensions placed inside the integrating sphere. All functions and goodness-of-fit statistics are calculated over the wavelength range 400–700 nm. R^2 is the coefficient of determination, and RMSE is the root mean square error between observed (O_i) and predicted (P_i) values of OD_s calculated as $[1/(N-m) \times \Sigma_{i=1}^{N}(P_i - O_i)^2]^{1/2}$. MNB is the mean normalized bias in percent, calculated as $100/N \times \Sigma_{i=1}^{N}(P_i - O_i/O_i)$. NRMS represents the normalized root mean square error (in percent) calculated as $\{100/(N-1) \times \Sigma_{i=1}^{N}[(P_i - O_i)/O_i - \mathrm{MNB}/100]^2\}^{1/2}$. N is the number of paired observations used in computing the error statistics, and m the number of coefficients in the fit.

in OD_s measured with different samples inside sphere remain fairly constrained across the examined range of OD_f obtained from the IS method [Fig. 8(e)], the extent of such variations is much larger when OD_s was measured outside sphere [Fig. 8(f)]. For example, for OD_f values of 0.1, 0.2, 0.3, and 0.4, the ratios of maximum to minimum OD_s from inside-sphere measurements are 1.51, 1.33, 1.16, and 1.04, respectively. For the outside-sphere measurements of OD_s these ratios are significantly higher, namely 2.44, 1.50, 1.39, and 1.24.

The results in Fig. 8 also indicate that the sample-to-sample variability in the OD_s versus OD_f relationship is significantly smaller for the optimal methodological scenario in which both OD_f and OD_s were measured inside the integrating sphere [Fig. 8(e)] compared with the analogous relationships for the T [Fig. 8(a)] and T-R [Fig. 8(c)] filter-pad methods. This comparative analysis supports the notion of the superiority of the IS over T and T-R filter-pad methods, which is consistent with the findings of a previous study [32]. Both the quadratic and power functions were examined for fitting the data of OD_s versus OD_f for the IS method presented in Fig. 8(e), which showed that the power function provides a somewhat better fit than the quadratic function (Table 4). This slight improvement of goodness-of-fit with the power function is consistent with our results from EXPT1 for the T and T-R methods. We recommend the use of the power function for the IS method as the best approach for pathlength amplification correction for this method. This formula is given in Table 4 and the function is also plotted in Fig. 8(e).

Although the measurements with the T and T-R methods in EXPT2 were limited in number and not intended for

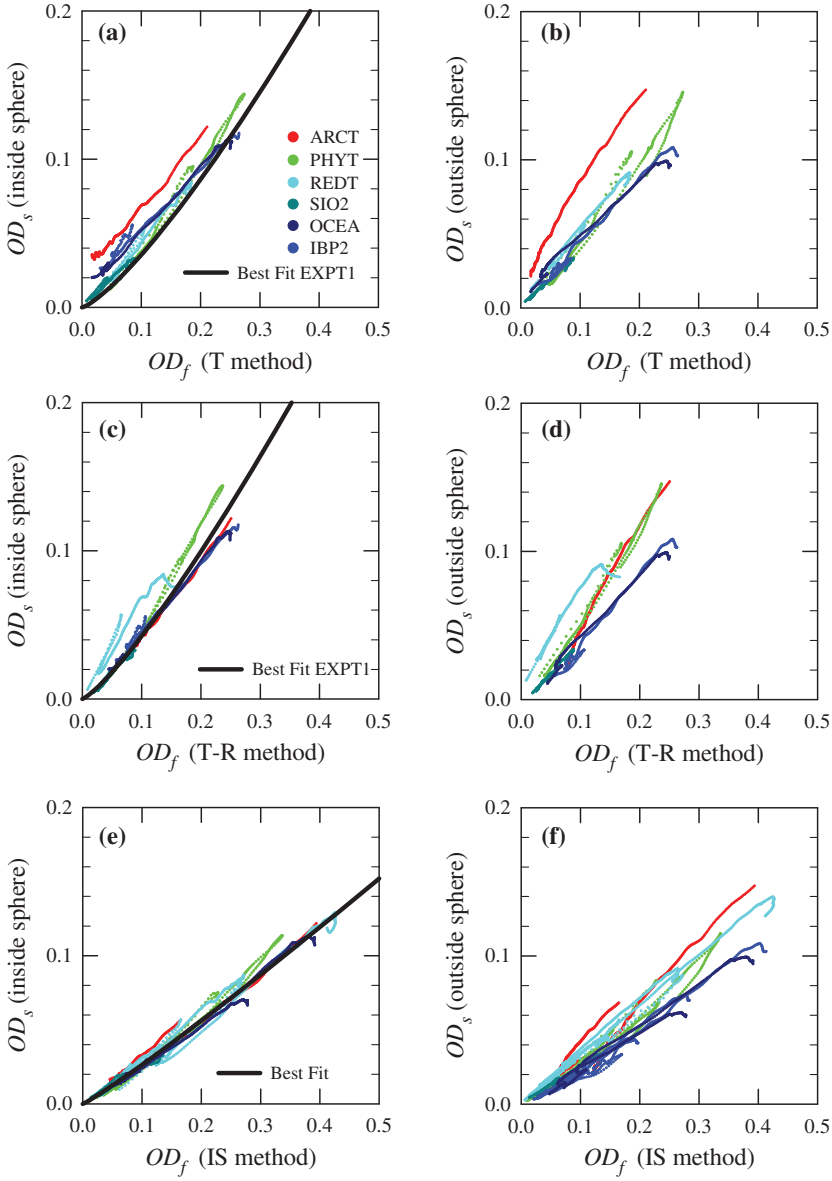

Fig. 8. Relationships between OD_s and OD_f obtained for EXPT2 samples using three configurations for the measurement of OD_f, the T method [(a), (b)], the T-R method [(c), (d)], and the IS method [(e), (f)], and two configurations for the measurement of OD_s as described in the caption of Fig. 7. The symbol legend provided in panel (a) is applicable to all six panels. For panel (e), the best fit power function to the data is indicated (Table 4). In panels (a) and (c), the best fit power functions obtained from EXPT1 are shown for comparison.

establishing the functional relationships $OD_s = f(OD_f)$, these data provide important insights about the performance limitations of these methods. We recall that in contrast to EXPT1, the inside-sphere measurements of OD_s in EXPT2 were not null-point corrected because some samples exhibited significant absorption in the NIR spectral range. However, the null-point correction was applied to the filter-pad measurements with the T method because in this method it is not possible to discriminate between the methodological error and potential presence of true absorption signal in the NIR. As a result, the OD_s versus OD_f data for the T method show large differences among the samples with a characteristic leftward shift of data for samples with significant NIR absorption compared with samples with no or very small NIR absorption [Fig. 8(a)]. This shift is particularly well pronounced over a broader range of OD_f for the ARCT sample and also at low values of OD_f (less than approximately 0.1) for IBP2 and OCEA. For comparison, Fig. 8(a) also includes our recommended power function fit for the T method obtained from EXPT1. Recall that the samples in EXPT1 exhibited no significant NIR absorption, and both the inside-sphere measurements of OD_s and the T measurements of OD_f were null-point corrected. Fig. 8(a) demonstrates that the use of the T method with the recommended power function for samples such as ARCT can lead to large errors in pathlength amplification correction. For example, the power function would underestimate the values of OD_s (and hence the particulate absorption coefficient) for ARCT by 48 and 25% for the measured OD_f of 0.1 and 0.2, respectively.

Whereas the T-R method is generally expected to perform better for a wide range of samples than the T method, our results from EXPT2 also provide evidence for the possible presence of significant trend outliers in the relationship between OD_s and OD_f for the T-R method [Fig. 8(c)]. In particular, the data for the REDT and partly for PHYT do not conform to the pattern created by other samples and also the recommended power function fit obtained from EXPT1. For example, the power function would underestimate OD_s for the REDT sample by 38% for the OD_f of 0.1. Note also that the T-R data in Fig. 8(c), which were not null-point corrected, show smaller variability and more consistent behavior for the different samples at low OD_f values compared with the T data [Fig. 8(a)]. This result is expected because the T-R method was developed to minimize the scattering error and enable more accurate measurement of weak absorption at the long-wavelength end of the visible spectrum and NIR.

Our recommended representations of the OD_s versus OD_f relationship as power functions for the T, T-R, and IS methods are compared with previously established relationships in Fig. 9. More than 10 historical relationships are available for the T method, and almost all of them were obtained from measurements of phytoplankton cultures. These data show large variability corresponding to as much as approximately threefold variation in the pathlength amplification factor β at some OD_f values [Fig. 9(a)]. Our recommended relationship is located near the middle of the presented set of curves. In terms of proximity over the broad range of OD_f values our relationship is closest to those of [9,51], and one curve of [64] which was obtained for the culture of *Phaeodactylum tricornutum*. The lowest outliers among the relationships corresponding to the highest values of β represent the determinations for the cultures of *Synechococcus* and *Prochlorococcus* by [50] and [64]. The highest outliers with generally lowest values of β, especially for relatively high OD_f values, are from the study of [65] and [24]. We also note that a considerable portion of variability among the literature data shown in Fig. 9(a) is likely caused by poor measurement geometry for determining OD_s as demonstrated by our results obtained with the T method [Figs. 7(a) and 7(b) and Figs. 8(a) and 8(b)]. No historical data of OD_s presented in Fig. 9(a) were obtained with the inside-sphere configuration of measurement.

Although the availability of literature data for the T-R and IS methods is very limited, the agreement between these data and the power function relationships established in the present study for these two methods is very good [Figs. 9(b) and 9(c)]. This agreement supports our recommendation for the use of our relationships for the T-R and IS methods. The advantage of using our relationship for the T-R method over the original relationship proposed by [26] is that this previous relationship was based on measurements with a single phytoplankton species, *Scenedesmus obliquus*, as opposed to our study of a number of samples characterized by a wide range of particulate composition. We note, however, that the consistency of the original Tassan and Ferrari relationship with data for natural seawater samples from the Adriatic Sea was demonstrated earlier by [38]. With regard to the IS method, the primary advantage of using our relationship stems from the fact that the other relationship proposed by Röttgers and Gehnke [32] is discontinuous at $OD_f = 0.1$, and these investigators did not provide an explicit relationship in the form of $OD_s = f(OD_f)$. In addition, although our relationship is based on measurements on much smaller number of samples than the Röttgers and Gehnke relationship, a wide range of particulate composition in our samples was characterized by ancillary measurements, and no specific type of particulate composition has had a dominant statistical weight in establishing our relationship. This aspect is unclear in the case of the study by Röttgers and Gehnke because no ancillary measurements were made to characterize the samples beyond their absorption spectra.

Although large and diverse sets of independent data for validating our power function fits are not available, it is useful to provide statistical parameters characterizing differences between OD_s predicted from the power function fits and the measured OD_s as presented in Fig. 7(a) for the T method, Fig. 7(c) for the T-R method, and Fig. 8(e) for the IS method. These statistical parameters and the formulas for calculating the parameters are given in Table 5. Note that although these calculations were made for OD_s, some of the presented parameters can be interpreted as uncertainties in the determinations of particulate absorption coefficient, $a_p(\lambda)$, produced by pathlength amplification correction with the recommended power functions. For example, the median ratio of predicted to measured values of OD_s, MR, provides a measure of bias, and the median absolute percent difference between the predicted and measured OD_s, MPD, is a measure of random error. Overall, the error statistics are very good for the three methods, but

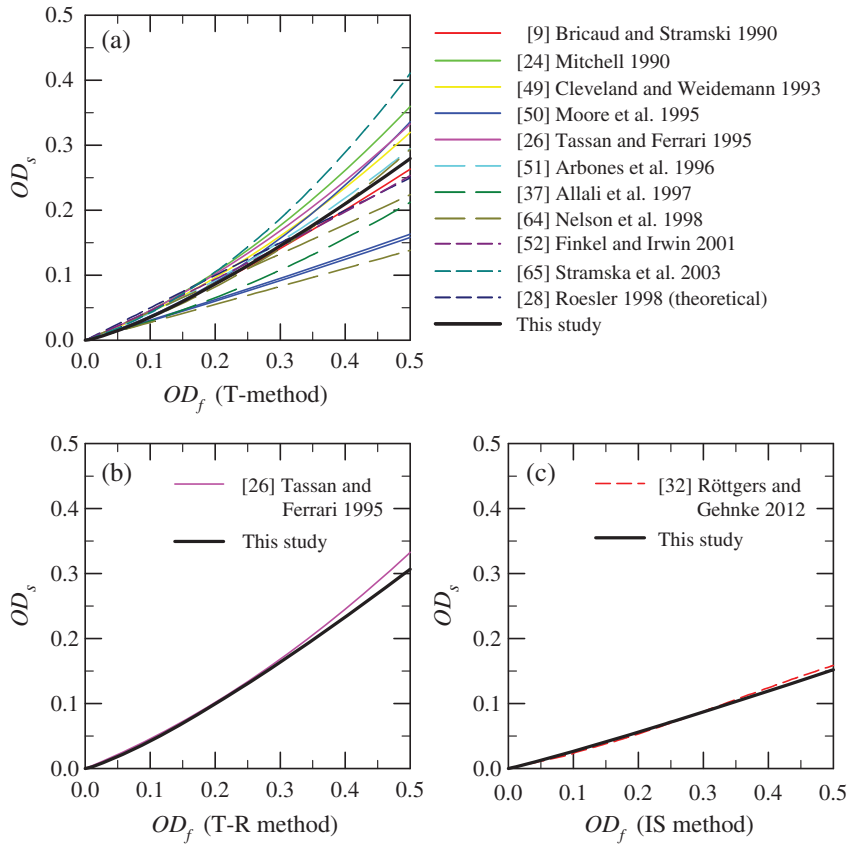

Fig. 9. Comparison of the relationships between OD_s and OD_f obtained in this study with other relationships in the literature: (a) OD_f obtained with the T method; (b) OD_f obtained with the T-R method; (c) OD_f obtained with the IS method.

there are also some noticeable differences between the methods. The best error statistics are for the IS method, and the largest errors are for the T method. For example, MR for the IS method is 1.011 which corresponds to a very small positive bias of only 1.1%. For the T method, it is 0.967 (negative bias of 3.3%). A similar tendency is observed for MPD which is 7.13% for the IS method and 8.84% for the T method. It is important to re-emphasize that these statistics are based on the comparison of predicted values of OD_s with the measured values of OD_s which were used for fitting the functions. This certainly resulted in some error reduction compared with the errors expected from similar analysis with independent data of measured OD_s. This is supported by additional error statistics presented in Table 5 (the numbers in parenthesis) for the T and T-R methods, which are based on the comparison of OD_s predicted from the power functions established in EXPT1 with the measured OD_s from EXPT2 [Figs. 8(a) and 8(c)]. Although the independent data of T and T-R measurements from EXPT2 are rather limited in size, they provide clear evidence for higher predictive uncertainty of our recommended power function fits from EXPT1, especially for the T method. For this method the bias increased to approximately −27%

Table 5. Error Statistics for the Comparison of Measured OD_s with OD_s Computed Using the Fitted Power Functions Shown in Table 4[a]

Method	MB	MR	SIQR	MPD (%)	RMSD	N
T	−0.00023	0.967	0.0864	8.84	0.00826	11137
	(−0.01153)	(0.734)	(0.2012)	(26.64)	(0.01535)	(1806)
T-R	−0.00018	0.980	0.0769	7.07	0.00682	11137
	(−0.00223)	(0.998)	(0.1037)	(9.14)	(0.00998)	(1806)
IS	0.00002	1.011	0.0700	7.13	0.00351	5117

[a]Statistics for the T and T-R methods are computed from EXPT1, and for the IS method data from EXPT2 are used. For the T and T-R methods, the numbers in parentheses represent the error statistics when the power function determined from EXPT1 is applied to independent measurements made in EXPT2. MB represents the mean bias calculated as the average difference between observed (O_i) and predicted (P_i) values of OD_s. MR represents the median ratio of P_i/O_i, and SIQR is the semi-interquartile range of this ratio calculated as SIQR = (Q3 − Q1)/2, where Q1 is the 25th percentile and Q3 is the 75th percentile. MPD is the median absolute percent difference representing the median of the individual absolute percent differences, $PD_i = 100(|P_i - O_i|/O_i)$. RMSD is the root mean square deviation and calculated as $[1/(N) \times \Sigma_{i=1}^{N}(P_i - O_i)^2]^{1/2}$. N is the number of observations used in computing the error statistics.

(MR = 0.73) and MPD to approximately 27%. For the T-R method, the changes are much smaller as the bias did not increase and MPD increased slightly to 9.15% compared with the result of 7.07% based entirely on EXPT1.

For the IS method we have no independent data to provide additional insight into potential uncertainties produced by variation in pathlength amplification but in an earlier study [32] a maximum error of 14% was reported for natural seawater samples. Our estimate of MPD (Table 5) indicates that 50% of our IS data points presented in Fig. 8(e) would be predicted from the power function with an error larger than 7.1% which is about half of the maximum error reported by [32]. Our calculations (not reported in Table 5) also indicate that 95% of our data would be in error smaller than 25.3% with maximum errors never exceeding 65%. Note that the small proportion of data subject to relatively large errors tends to correspond to relatively low values of the measured OD_f which in turn correspond to spectral regions with relatively weak absorption. If we restrict OD_f to values larger than 0.1 then the maximum error is reduced to 33%, and 95% of these data have an error smaller than 20%. For the data with $OD_f > 0.2$, these error estimates are further reduced to 20.9% and 13.1%.

5. CONCLUSIONS

In this paper, we analyzed data from special experiments that were conducted with a purpose to establish consensus protocols for the pathlength amplification correction in routine measurements of absorption coefficient of aquatic particles within the visible spectral range with the T, T-R, and IS methods of the filter-pad technique. The key aspect of the experimental design was to perform a comprehensive set of concomitant measurements of absorption spectra with different filter-pad methods and reference absorption measurements on particle suspensions with different geometric configurations for a number of carefully selected samples characterized by a wide range of particulate composition from mineral-dominated to phytoplankton-dominated including several intermediate cases. Considering the current state of knowledge and the scope of the available database, this approach has been chosen as most advantageous for advancing the pathlength amplification correction toward consensus protocols.

The main results of this study include the functional relationships between OD_s and OD_f which are recommended for the pathlength amplification correction of filter-pad measurements with the T, T-R, and IS methods. The recommended relationships have the form of power functions (Table 4). Our results also support the notion that the filter-pad methods can be ranked in descending order of superiority as follows: IS, T-R, and T (Table 5). As the best IS method is not yet in widespread use we recommend that concerted efforts be undertaken by aquatic scientists involved in measurements of particulate absorption toward accepting the IS method as a standard variant of the filter-pad technique, and thus replacing the current standard T method. The IS method has more stringent requirements with regard to the spectrophotometer equipment than the T and T-R methods. Specifically, a sufficiently large integrating sphere that can accommodate a sample inside the sphere is required; in practice it is desirable to have a sphere at least 15 cm in diameter. Nevertheless, the benefits from improved accuracy and precision of measurements with the IS method far outweigh the additional equipment cost that may be incurred in comparison with the use of no integrating sphere in the T method or relatively small integrating sphere in the T and T-R methods. It is also beneficial that the protocol of IS measurements is fairly simple, not more laborious than the T protocol, and significantly less labor-intensive and time-consuming than the T-R protocol.

Because it is expected that the T method will continue to be used for some time despite its lower accuracy and precision, we recommend a new power function relationship between OD_s and OD_f for the pathlength amplification correction for this method. This formulation falls in the middle range of relationships reported in the literature. In cases when the T method is the only available option for measuring particulate absorption, this method should be restricted to the use on samples with no or nearly undetectable absorption in the NIR spectral range. We strongly caution against using the T method for samples with significant absorption in the NIR because no reliable pathlength amplification correction can be formulated for such samples. The use of inappropriate pathlength amplification formula for such samples can lead to unacceptably large errors (>50%) in determination of the particulate absorption coefficient from the T method. For this type of samples, the T-R method with our recommended power function for pathlength amplification correction can be used as a second choice option if the IS method is not available. Recall, however, that over the last 20 years since its inception, the T-R method was used much less frequently than the T method primarily because of a more demanding protocol of measurements. Therefore, whereas the T-R method can remain as a viable option, especially under certain circumstances associated with specific types of samples and available spectrophotometric equipment, this method is not expected to gain widespread use for routine measurements. A broad implementation of the IS method as a standard variant of the filter-pad technique appears to be the most desirable pathway for achieving the optimum quality of routine measurements of hyperspectral particulate absorption coefficient on discrete aquatic samples. Whereas very good quantitative data can now be obtained with this method in the visible spectral range, one important methodological problem that requires special attention in future research is the improvement of measurement and quantification of particulate absorption in the UV spectral region.

Funding. National Aeronautics and Space Administration (NASA) (NNX15AC55G).

Acknowledgment. We thank J. Ehn for assistance in laboratory work and two anonymous reviewers for comments on the manuscript.

REFERENCES

1. C. S. Yentsch, "A non-extractive method for the quantitative estimation of chlorophyll in algal cultures," Nature **179**, 1302–1304 (1957).
2. C. S. Yentsch, "Measurement of visible light absorption by particulate matter in the ocean," Limnol. Oceanogr. **7**, 207–217 (1962).

3. H. Trüper and C. S. Yentsch, "Use of glass-fiber filters for the rapid preparation of in vivo absorption spectra of photosynthetic bacteria," J. Bacteriol. **94**, 1255–1256 (1967).
4. E. S. Fry, G. W. Kattawar, and R. M. Pope, "Integrating cavity absorption meter," Appl. Opt. **31**, 2055–2065 (1992).
5. J. T. O. Kirk, "Point-source integrating-cavity absorption meter: theoretical principles and numerical modeling," Appl. Opt. **36**, 6123–6128 (1997).
6. R. Röttgers, C. Häse, and R. Doerffer, "Determination of particulate absorption of microalgae using a point source integrating cavity absorption meter," Limnol. Oceanogr. Methods **5**, 1–12 (2007).
7. M. Kishino, M. Takahashi, N. Okami, and S. Ichimura, "Estimation of the spectral absorption coefficient of phytoplankton in the sea," Bull. Mar. Sci. **37**, 634–642 (1985).
8. G. M. Ferrari and S. Tassan, "A method using chemical oxidation to remove light absorption by phytoplankton pigments," J. Phycol. **35**, 1090–1098 (1999).
9. A. Bricaud and D. Stramski, "Spectral absorption coefficients of living phytoplankton and nonalgal biogenous matter: a comparison between Peru upwelling area and the Sargasso Sea," Limnol. Oceanogr. **35**, 562–582 (1990).
10. J. S. Cleveland and M. J. Perry, "A model for partitioning particulate absorption into phytoplanktonic and detrital components," Deep Sea Res. Part I **41**, 197–221 (1994).
11. G. Zheng and D. Stramski, "A model for partitioning the light absorption coefficient of suspended marine particles into phytoplankton and nonalgal components," J. Geophys. Res. Oceans **118**, 2977–2991 (2013).
12. M. R. Lewis, J. J. Cullen, and T. Platt, "Phytoplankton and thermal structure in the upper ocean: consequences of nonuniformity in chlorophyll profile," J. Geophys. Res. **88**, 2565–2570 (1983).
13. N. Hoepffner and S. Sathyendranath, "Determination of the major groups of phytoplankton pigments from the absorption spectra of total particulate matter," J. Geophys. Res. **98**, 22789–22803 (1993).
14. A. M. Ciotti, M. R. Lewis, and J. J. Cullen, "Assessment of the relationships between dominant cell size in natural phytoplankton communities and the spectral shape of the absorption coefficient," Limnol. Oceanogr. **47**, 404–417 (2002).
15. J. Marra, C. Trees, and J. O'Reilly, "Phytoplankton pigment absorption: a strong predictor of primary productivity in the surface ocean," Deep Sea Res. Part I **54**, 155–163 (2007).
16. E. Torrecilla, D. Stramski, R. A. Reynolds, E. Millán-Núñez, and J. Piera, "Cluster analysis of hyperspectral optical data for discriminating phytoplankton pigment assemblages in the open ocean," Rem. Sens. Environ. **115**, 2578–2593 (2011).
17. K. L. Carder, F. R. Chen, Z. P. Lee, S. K. Hawes, and D. Kamykowski, "Semianalytic Mmoderate-Rresolution Iimaging Sspectrometer algorithms for chlorophyll and absorption with bio-optical domains based on nitrate-depletion temperatures," J. Geophys. Res. **104**, 5403–5421 (1999).
18. H. Loisel and D. Stramski, "Estimation of the inherent optical properties of natural waters from irradiance attenuation coefficient and reflectance in the presence of Raman scattering," Appl. Opt. **39**, 3001–3011 (2000).
19. Z. P. Lee, K. L. Carder, and R. A. Arnone, "Deriving inherent optical properties from water color: a multiband quasi-analytical algorithm for optically deep waters," Appl. Opt. **41**, 5755–5772 (2002).
20. S. Maritorena, D. A. Siegel, and A. R. Peterson, "Optimization of a semianalytical ocean color model for global-scale applications," Appl. Opt. **41**, 2705–2714 (2002).
21. D. A. Kiefer and J. B. SooHoo, "Spectral absorption by marine particles of coastal waters of Baja California," Limnol. Oceanogr. **27**, 492–499 (1982).
22. J. C. Goldman and M. R. Dennet, "Susceptibility of some marine phytoplankton species to cell breakage during filtration and postfiltration rinsing," J. Exp. Mar. Biol. Ecol. **86**, 47–58 (1985).
23. H. Maske and H. Haardt, "Quantitative in vivo absorption spectra of phytoplankton: detrital absorption and comparison with fluorescence excitation spectra," Limnol. Oceanogr. **32**, 620–633 (1987).
24. B. G. Mitchell, "Algorithm for determining the absorption coefficient of aquatic particulates using the quantitative filter technique (QFT)," Proc. SPIE **1302**, 137–148 (1990).
25. D. Stramski, "Artifacts in measuring absorption spectra of phytoplankton collected on a filter," Limnol. Oceanogr. **35**, 1804–1809 (1990).
26. S. Tassan and G. M. Ferrari, "An alternative approach to absorption measurements of aquatic particles retained on filters," Limnol. Oceanogr. **40**, 1358–1368 (1995).
27. S. Tassan and G. M. Ferrari, "A sensitivity analysis of the 'transmittance-reflectance' method for measuring light absorption by aquatic particles," J. Plankton Res. **24**, 757–774 (2002).
28. C. S. Roesler, "Theoretical and experimental approaches to improve the accuracy of particulate absorption coefficients derived from the quantitative filter technique," Limnol. Oceanogr. **43**, 1649–1660 (1998).
29. H. M. Sosik, "Storage of marine particulate samples for light absorption measurements," Limnol. Oceanogr. **44**, 1139–1141 (1999).
30. S. E. Lohrenz, "A novel theoretical approach to correct for pathlength amplification and variable sampling loading in measurements of particulate spectral absorption by quantitative filter technique," Journal of plankton research **22**, 639–657 (2000).
31. I. Laurion, F. Blouin, and S. Roy, "The quantitative filter technique for measuring phytoplankton absorption: interference by MAAs in the UV waveband," Limnol. Oceanogr. Methods **1**, 1–9 (2003).
32. R. Röttgers and S. Gehnke, "Measurement of light absorption by aquatic particles: improvement of the quantitative filter technique by use of an integrating sphere approach," Appl. Opt. **51**, 1336–1351 (2012).
33. G. Neukermans, R. A. Reynolds, and D. Stramski, "Contrasting inherent optical properties and particle characteristics between an under-ice phytoplankton bloom and open water in the Chukchi Sea," Deep Sea Res. Part II **105**, 59–73 (2014).
34. G. Zheng, D. Stramski, and R. A. Reynolds, "Evaluation of the quasi-analytical algorithm for estimating the inherent optical properties of seawater from ocean color: comparison of Arctic and lower-latitude waters," Rem. Sens. Environ. **155**, 194–209 (2014).
35. W. L. Butler, "Absorption of light by turbid samples," J. Opt. Soc. Am. **52**, 292–299 (1962).
36. S. Tassan and G. M. Ferrari, "Measurement of light absorption by aquatic particles retained on filters: determination of the optical pathlength amplification by the 'transmittance-reflectance' method," J. Plankton Res. **20**, 1699–1709 (1998).
37. K. Allali, A. Bricaud, and H. Claustre, "Spatial variations in chlorophyll-specific absorption coefficients of phytoplankton and photosynthetically active pigments in the equatorial Pacific,." J. Geophys. Res. **102**, 12413–12423 (1997).
38. S. Tassan, G. M. Ferrari, A. Bricaud, and M. Babin, "Variability of the amplification factor of light absorption by filter-retained aquatic particles in the coastal environment," J. Plankton Res. **22**, 659–668 (2000).
39. B. G. Mitchell, M. Kahru, J. Wieland, and M. Stramska, "Determination of spectral absorption coefficients of particles, dissolved material and phytoplankton for discrete water samples," in Ocean Optics Protocols for Satellite Ocean Color Sensor Validation, Rev. 4, Vol. IV: Inherent Optical Properties: Instruments, Characterizations, Field Measurements and Data Analysis Protocols, J. L. Mueller, G. S. Fargion, and C. R. McClain, eds. (NASA Goddard Space Flight Center, NASA/TM-2003-211621/Rev4-Vol. IV, 2003), pp. 39–64.
40. S. Tassan and G. M. Ferrari, "Variability of light absorption by aquatic particles in the near-infrared spectral region," Appl. Opt. **42**, 4802–4810 (2003).
41. M. Babin and D. Stramski, "Variations in the mass-specific absorption coefficient of mineral particles suspended in water," Limnol. Oceanogr. **49**, 756–767 (2004).
42. D. G. Bowers and C. E. Binding, "The optical properties of mineral suspended particles: a review and synthesis," Estuar. Coast. Shelf Sci. **67**, 219–230 (2006).
43. D. Stramski, S. B. Woźniak, and P. J. Flatau, "Optical properties of Asian mineral dust suspended in seawater," Limnol. Oceanogr. **49**, 749–755 (2004).
44. D. Stramski, M. Babin, and S. B. Woźniak, "Variations in the optical properties of terrigeneous mineral-rich particulate matter suspended in seawater," Limnol. Oceanogr. **52**, 2418–2433 (2007).

45. R. Röttgers, C. Dupouy, B. B. Taylor, A. Bracher, and S. B. Woźniak, "Mass-specific light absorption coefficients of natural aquatic particles in the near-infrared spectral region," Limnol. Oceanogr. **59**, 1449–1460 (2014).
46. N. B. Nelson and B. B. Prézelin, "Calibration of an integrating sphere for determining the absorption coefficient of scattering suspensions," Appl. Opt. **32**, 6710–6717 (1993).
47. M. Babin and D. Stramski, "Light absorption by aquatic particles in the near-infrared spectral region," Limnol. Oceanogr. **47**, 911–915 (2002).
48. S. G. H. Simis, S. W. M. Peters, and H. J. Gons, "Remote sensing of the cyanobacterial pigment phycocyanin in turbid inland water," Limnol. Oceanogr. **50**, 237–245 (2005).
49. J. S. Cleveland and A. D. Weidemann, "Quantifying absorption by aquatic particles: a multiple scattering correction for glass-fiber filters," Limnol. Oceanogr. **38**, 1321–1327 (1993).
50. L. R. Moore, R. Goericke, and S. W. Chisholm, "Comparative physiology of *Synechococcus* and *Prochlorococcus*: influence of light and temperature on growth, pigments, fluorescence and absorptive properties," Mar. Ecol. Prog. Ser. **116**, 259–275 (1995).
51. B. Arbones, F. G. Figueiras, and M. Zapata, "Determination of phytoplankton absorption coefficient in natural seawater samples: evidence of a unique equation to correct the pathlength amplification of glass-fiber filters," Mar. Ecol. Prog. Ser. **137**, 293–304 (1996).
52. Z. V. Finkel and A. J. Irwin, "Light absorption by phytoplankton and the filter amplification correction: cell size and species effects," J. Exp. Mar. Biol. Ecol. **259**, 51–61 (2001).
53. A. Bricaud, A.-L. Bedhomme, and A. Morel, "Optical properties of diverse phytoplanktonic species: experimental results and theoretical predictions," J. Plankton Res. **10**, 851–873 (1988).
54. D. Stramski and J. Piskozub, "Estimation of scattering error in spectrophotometric measurements of light absorption by aquatic particles from three-dimensional radiative transfer simulations," Appl. Opt. **42**, 3634–3646 (2003).
55. K. R. Arrigo, D. K. Perovich, R. S. Pickart, Z. W. Brown, G. L. van Dijken, K. E. Lowry, M. M. Mills, M. A. Palmer, W. M. Balch, N. R. Bates, C. R. Benitez-Nelson, E. Brownlee, K. E. Frey, S. R. Laney, J. Mathis, A. Matsuoka, B. G. Mitchell, G. W. K. Moore, R. A. Reynolds, H. M. Sosik, and J. H. Swift, "Phytoplankton blooms beneath the sea ice in the Chukchi sea," Deep Sea Res. Part II **105**, 1–16 (2014).
56. A. Knap, A. Michaels, A. Close, H. Ducklow, and A. Dickson (eds.), Protocols for the Joint Global Ocean Flux Study (JGOFS) Core Measurements (JGOFS Report No. 19, 1996) [Reprint of the IOC Manuals and Guides No. 29, UNESCO, Paris, 1994].
57. D. W. Van der Linde, Protocol for determination of total suspended matter in oceans and coastal zones, Technical Note No. 1.98.182 (CEC-JRC, 1998).
58. D. Stramski, R. A. Reynolds, M. Babin, S. Kaczmarek, M. R. Lewis, R. Röttgers, A. Sciandra, M. Stramska, M. S. Twardowski, B. A. Franz, and H. Claustre, "Relationships between the surface concentration of particulate organic carbon and optical properties in the eastern South Pacific and eastern Atlantic Oceans," Biogeosciences **5**, 171–201 (2008).
59. S. B. Woźniak, D. Stramski, M. Stramska, R. A. Reynolds, V. M. Wright, E. Y. Miksic, M. Cichocka, and A. M. Cieplak, "Optical variability of seawater in relation to particle concentration, composition, and size distribution in the nearshore marine environment at Imperial Beach, California," J. Geophys. Res. **115**, C08027 (2010), doi:10.1029/2009JC005554.
60. R. J. Ritchie, "Universal chlorophyll equations for estimating chlorophylls *a*, *b*, *c*, and *d* and total chlorophylls in natural assemblages of photosynthetic organisms using acetone, methanol, or ethanol solvents," Photosynthetica **46**, 115–126 (2008).
61. R. A. Reynolds, D. Stramski, V. M. Wright, and S. B. Woźniak, "Measurements and characterization of particle size distributions in coastal waters," J. Geophys. Res. **115**, C08024 (2010), doi:10.1029/2009JC005930.
62. C. J. Lorenzen and J. N. Downs, "The specific absorption coefficients of chlorophyllide *a* and pheophorbide *a* in 90% acetone, and comments on the fluorometric determination of chlorophyll and phaeopigments," Limnol. Oceanogr. **31**, 449–452 (1986).
63. A. Morel, "Diffusion de la lumière par les eaux de mer. Résultats experimentaux et approache théorique," in *Optics of the Sea*, NATO AGARD Lecture Series No. 61 (NATO, 1973), pp. 3.1-1–3.1-76.
64. N. B. Nelson, D. A. Siegel, and A. F. Michaels, "Seasonal dynamics of colored dissolved material in the Sargasso Sea," Deep Sea Res. Part 1 **45**, 931–957 (1998).
65. M. Stramska, D. Stramski, R. Hapter, S. Kaczmarek, and J. Stoń, "Bio-optical relationships and ocean color algorithms for the north polar region of the Atlantic," J. Geophys. Res. **108**, 3143 (2003), doi:10.1029/2001JC001195.
66. M. Stramska, D. Stramski, S. Kaczmarek, D. B. Allison, and J. Schwarz, "Seasonal and regional differentiation of bio-optical properties within the north polar Atlantic," J. Geophys. Res. **111**, C08003 (2006), doi:10.1029/2005JC003293.